PNAS RESEARCH ARTICLE | ECOLOGY APPLIED MATHEMATICS OPEN ACCESS

Rate-induced tipping in complex high-dimensional ecological networks

Shirin Panahi[a], Younghae Do[b], Alan Hastings[c,d], and Ying-Cheng Lai[a,e,1]

Edited by Nils Stenseth, Universitetet i Oslo, Oslo, Norway; received May 25, 2023; accepted November 15, 2023

In an ecosystem, environmental changes as a result of natural and human processes can cause some key parameters of the system to change with time. Depending on how fast such a parameter changes, a tipping point can occur. Existing works on rate-induced tipping, or R-tipping, offered a theoretical way to study this phenomenon but from a local dynamical point of view, revealing, e.g., the existence of a critical rate for some specific initial condition above which a tipping point will occur. As ecosystems are subject to constant disturbances and can drift away from their equilibrium point, it is necessary to study R-tipping from a global perspective in terms of the initial conditions in the entire relevant phase space region. In particular, we introduce the notion of the probability of R-tipping defined for initial conditions taken from the whole relevant phase space. Using a number of real-world, complex mutualistic networks as a paradigm, we find a scaling law between this probability and the rate of parameter change and provide a geometric theory to explain the law. The real-world implication is that even a slow parameter change can lead to a system collapse with catastrophic consequences. In fact, to mitigate the environmental changes by merely slowing down the parameter drift may not always be effective: Only when the rate of parameter change is reduced to practically zero would the tipping be avoided. Our global dynamics approach offers a more complete and physically meaningful way to understand the important phenomenon of R-tipping.

tipping point | rate-induced tipping | mutualistic networks | nonlinear dynamics | scaling law

Significance

Human activities are having increasingly negative impacts on natural systems, and it is of interest to understand how the "pace" of parameter change may lead to catastrophic consequences. This work studies the phenomenon of rate-induced tipping (R-tipping) in high-dimensional ecological networks, where the rate of parameter change can cause the system to undergo a tipping point from healthy survival to extinction. A quantitative scaling law between the probability of R-tipping and the rate was uncovered, with a striking and devastating consequence: In order to reduce the probability, parameter changes must be slowed down to such an extent that the rate practically reaches zero. This may pose an extremely significant challenge in our efforts to protect and preserve the natural environment.

In complex dynamical systems, the phenomenon of tipping point, characterized by an abrupt transition from one type of behavior (typically normal, healthy, or survival) to another type (e.g., catastrophic), has received growing attention (1–25). A tipping point is often of significant concern because it is a point of "no return" in the parameter space, manifested by the collapse of the system as a parameter passes through a critical value. In ecological systems, sudden extinction of species on a large scale can be the result of a tipping point (1–4). Tipping points can arise in diverse contexts such as the outbreak of epidemics (26), global climate changes (27), and the sudden transition from normal to depressed mood in bipolar patients (28). In nonlinear dynamics, a common type of bifurcation responsible for a tipping point is saddle-node bifurcations (forward or backward). Consider the situation where, in the parameter regime of interest, there are two coexisting stable steady states: a "high" state corresponding to normal or "survival" functioning and a "low" or "extinction" state, each with its own basin of attractor. Suppose external factors such as climate change cause a bifurcation parameter of the system to increase. A tipping point is a backward saddle-node bifurcation, after which the "survival" fixed point disappears, leaving the "extinction" state as the only destination of the system, where the original basin of the "survival" state is absorbed into the basin of the "extinction" state.

In real-world dynamical systems, parameters are not stationary but constantly drift in time. A known example is the slow increase in the average global temperature with time due to human activities. In ecological systems, some key parameters such as the carrying capacity or the species decay rate can change with time, and there is a global tendency for such parameter changes to "speed up." In fact, the rate of environmental change is an important driver across different scales in ecology (29). The behavior of the parameter variations with time introduces another "meta" parameter into the dynamical process: the rate of change of the parameters. About 10 y ago, it was found that the rate can induce a tipping point—the phenomenon of rate-induced tipping or R-tipping (9), which is relevant to fields such as climate science (30, 31), neuroscience (32, 33), vibration engineering (34), and even competitive economy (35). Existing studies of R-tipping were for low-dimensional dynamical systems and the analysis approaches were "local" in the sense that they focused on the behaviors of some specific initial condition and trajectory,

Author contributions: A.H. and Y.-C.L. designed research; S.P. and Y.-C.L. performed research; Y.-C.L. contributed new reagents/analytic tools; S.P., Y.D., A.H., and Y.-C.L. analyzed data; and S.P. and Y.-C.L. wrote the paper.

The authors declare no competing interest.

This article is a PNAS Direct Submission.

[1]To whom correspondence may be addressed. Email: Ying-Cheng.Lai@asu.edu.

This article contains supporting information online at https://www.pnas.org/lookup/suppl/doi:10.1073/pnas.2308820120/-/DCSupplemental.

Published December 13, 2023.

addressing issues such as the critical rate for tipping (36, 37). In particular, with respect to a specific initial condition, R-tipping in these studies was defined as an abrupt change in the behavior of the system (or a critical transition) taking place at a specific rate of change of a bifurcation parameter (9).

The state that an ecological system is in depends on a combination of deterministic dynamics, small-scale stochastic influences, e.g., demographic stochasticity (38), and large stochastic disturbances such as drought or other significant climatic event (39). So when considering future dynamics of ecological systems, it makes sense to consider systems that may be far from equilibrium, but still within the basin of attraction of an equilibrium, rather than starting at the equilibrium. High-dimensional ecological systems are particularly likely to be found far from equilibrium. In fact, it has been suggested that it can be common for ecosystems to be in some transient state (40, 41).

In this paper, we focus on high-dimensional, empirical ecological networks and investigate R-tipping with two key time-varying parameters by presenting a computationally feasible, "global" approach to exploring the entire relevant phase space region with analytic insights. We focus on a representative class of such systems: mutualistic networks (14, 17, 19, 21, 42–48) that are fundamental to ecological systems, which are formed through mutually beneficial interactions between two groups of species. In a mutualistic network, a species in one group derives some form of benefit from the relationship with some species in the other group. Examples include the corals and the single-celled zooxanthellae that form the large-scale coral reefs and the various networks of pollinators and plants in different geographical regions of the world. These networks influence biodiversity, ecosystem stability, nutrient cycling, community resilience, and evolutionary dynamics (49), and they are a key aspect of ecosystem functioning with implications for conservation and ecosystem management. Understanding the ecological significance of mutualistic networks is crucial for unraveling the complexities of ecological communities and for implementing effective strategies to safeguard biodiversity and ecosystem health (50). Mathematically, because of the typically large number of species involved in the mutualistic interactions, the underlying networked systems are high-dimensional nonlinear dynamical systems.

We first ask whether R-tipping can arise in such high-dimensional systems by simulating a number of empirical pollinator-plant mutualistic networks (Table 1) and obtain an affirmative answer. Our computations reveal that the critical rate above which a tipping point occurs depends strongly on the initial condition. Rather than studying the critical rate for any specific initial condition, we go beyond the existing local analysis approaches by investigating the probability of R-tipping for a large ensemble of initial conditions taken from the whole relevant phase space and asking how this probability, denoted as $\Phi(r)$, depends on the rate r of parameter change. We find a scaling law between $\Phi(r)$ and r: As the rate increases, the probability first increases rapidly, then slowly, and finally saturates. Using a universal two-dimensional (2D) effective model that was validated to be particularly suitable for predicting and analyzing tipping points in high-dimensional mutualistic networks (17), we analytically derive the scaling law. Specifically, let $\kappa(t)$ be the parameter that changes with time linearly at the rate r in a finite range, denoted as $[\kappa_{\min}, \kappa_{\max}]$. The scaling law is given by:

$$\Phi(r) \sim \exp\left[-C(\kappa_{\max} - \kappa_{\min})/r\right], \qquad [1]$$

where $C > 0$ is a constant. Our theoretical analysis indicates that, for 2D systems, C is nothing but the maximum possible unstable eigenvalue of the mediating unstable fixed point on the boundary separating the basins of the survival and extinction attractors when the parameter κ varies in the range $[\kappa_{\min}, \kappa_{\max}]$. However, for high-dimensional systems, such correspondence does not hold, but C can be determined through a numerical fitting.

The scaling law Eq. **1** has the following features. First, the probability $\Phi(r)$ is an increasing function of r for $r > 0$ [$\Phi'(r) > 0$]. Second, $\Phi'(r)$ is a decreasing function of r, i.e., the increase of $\Phi(r)$ with r slows down with r and the rate of increase becomes zero for $r \to \infty$. Third, the rate of increase in $\Phi(r)$ with r is the maximum for $r \gtrsim 0$, and $\Phi(r)$ becomes approximately constant for $r > r^* \sim \sqrt{(\kappa_{\max} - \kappa_{\min})}$. This third feature has a striking implication because the probability of R-tipping will grow dramatically as soon as the rate of parameter change increases from zero. The real-world implication is alarming because it means that even a slow parameter change can lead to a system collapse with catastrophic consequences. To control or mitigate the environmental changes by merely slowing down the parameter drift may not always be effective: Only when the rate of parameter change is reduced to practically zero would the tipping be avoided!

Alternatively, the scaling law Eq. **1** can be expressed as the following explicit formula:

$$\Phi(r) = B\exp\left[-C(\kappa_{\max} - \kappa_{\min})/r\right], \qquad [2]$$

with an additional positive constant B. For 2D systems, B is the difference between the basin areas of the extinction state for $\kappa = \kappa_{\max}$ and $\kappa = \kappa_{\min}$. For high-dimensional systems, B can be determined numerically.

While a comprehensive understanding of the entire parameter space as well as the rates and directions of change associated with these parameters are worth investigating, the picture that motivated our work was the potential impacts of ongoing climate change on ecological systems. Under climate change, various parameters can vary in different directions, and some changes might offset the effects of others. Our focus is on the scenarios where the changes in parameters align with the observed detrimental environmental impacts. For example, consistent with environmental deterioration, in a mutualistic network the species decay rate can increase, and/or the mutualistic interaction strength can decrease. A simultaneous increase in the species decay rate and mutualistic strength does not seem physically reasonable in this context. We thus study scenarios of

Table 1. Empirical mutualistic networks studied in this work and their corresponding range of parameter change and fitting constants in Eq. 1

Network	Country	N_P	N_A	κ-interval	B	C
M_PL_008	Canary Islands	11	38	[0.90, 0.93]	0.36	0.19
M_PL_013	South Africa	9	56	[0.70, 0.99]	0.07	0.11
M_PL_022	Argentina	21	45	[0.75, 0.93]	0.88	0.12
M_PL_023	Argentina	23	72	[0.87, 0.96]	0.59	0.09
M_PL_027	New Zealand	18	60	[0.90, 0.95]	0.49	0.09
M_PL_032	USA	7	33	[0.82, 0.99]	0.55	0.19
M_PL_036	Açores	10	12	[0.74, 0.88]	0.39	0.12
M_PL_037	Denmark	10	40	[0.87, 0.93]	0.23	0.15
M_PL_038	Denmark	8	42	[0.85, 0.95]	0.30	0.15
M_PL_045	Greenland	17	26	[0.96, 0.98]	0.09	0.05

multiple parameter variations that align with the realistic climate change impacts by carrying out computations with a systematic analysis of the tipping-point transitions in the 2D parameter plane of the species decay rate and the mutualistic interaction strength.

Results

We consider the empirical mutualistic pollinator–plant networks from the Web of Life database (www.Web-of-Life.es). The needs to search for the parameter regions exhibiting R-tipping and to simulate a large number of initial conditions in the phase space as required by our global analysis approach as well as the high dimensionality of the empirical mutualistic networks demand extremely intensive computation (51). To make the computation feasible, we select ten networks to represent a diverse range of mutualistic interactions from different regions of the world and highlight the generality of our approach to R-tipping and the scaling law. The basic information about these networks such as the name of the networks, the countries where the empirical data were collected and the number of species in each network, is listed in Table 1. The dynamics of a mutualistic network of N_A pollinator and N_P plant species, taking into account the generic plant–pollinator interactions (42), can be described by a total of $N = N_A + N_P$ nonlinear differential equations of the Holling type (52) in terms of the species abundances as:

$$\dot{P}_i = P_i\left(\alpha_i^P - \sum_{l=1}^{N_p} \beta_{il}^P P_l + \frac{\sum_{j=1}^{N_A} \gamma_{ij}^P A_j}{1 + h\sum_{j=1}^{N_A} \gamma_{ij}^P A_j}\right), \qquad [3a]$$

$$\dot{A}_j = A_j\left(\alpha_j^A - \kappa_j - \sum_{l=1}^{N_A} \beta_{jl}^A A_l + \frac{\sum_{i=1}^{N_P} \gamma_{ji}^A P_i}{1 + h\sum_{i=1}^{N_P} \gamma_{ji}^A P_i}\right), \qquad [3b]$$

where P_i and A_j are the abundances of the i^{th} and j^{th} plant and pollinator species, respectively, $i = 1, \ldots, N_P$, $j = 1, \ldots, N_A$, κ is the pollinator decay rate, $\alpha^{P(A)}$ is the intrinsic growth rate in the absence of intraspecific competition and any mutualistic effect, h is the half-saturation constant. Intraspecific and interspecific competition of the plants (pollinators) is characterized by the parameters β_{ii}^P (β_{jj}^A) and β_{il}^P (β_{jl}^A), respectively. The mutualistic interactions as characterized by the parameter γ_{ij}^P can be written as $\gamma_{ij}^P = \xi_{ij}\gamma_0/K_i^\tau$, where $\xi_{ij} = 1$ if there is a mutualistic interaction between the i^{th} plant and j^{th} pollinator (zero otherwise), γ_0 is a general interaction parameter, K_i is the degree of the i^{th} plant species in the network, and τ determines the strength of the trade-off between the interaction strength and the number of interactions. (The expression for γ_{ji}^A is similar.)

The computational setting of our study is as follows. In the network system described by Eqs. **3a** and **3b**, the number of the equations determines the phase-space dimension of the underlying nonlinear dynamical system. There are a large number of basic parameters in the model, such as γ that quantifies the strength of the mutualistic interactions and κ characterizing the species decay rate. In the context of R-tipping, while all the parameters should be time-varying in principle, to make our study computationally feasible, we assume that the two key parameters (κ and γ) are time-dependent while keeping the other parameters fixed. Since the defining characteristic of a system exhibiting a tipping point is the coexistence of two stable steady states: survival and extinction, we focus on the range of parameter variations in which the network system under study exhibits the two stable equilibria. When presenting our results (Fig. 1 below and *SI Appendix*, Figs. S4–S14), in each case, the parameter variation is along a specific direction in the 2D parameter plane: κ and γ with the goal to understand how changes in these two parameters impact the R-tipping probability.

To introduce the rate change of a parameter, we consider the scenario where negative environmental impacts cause the species decay rate to increase linearly with time at the rate r from a minimal value $\kappa_{\min}$ to a maximal value $\kappa_{\max}$:

$$\dot{\kappa}_j = \begin{cases} r & \text{if } \kappa_{\min} < \kappa_j < \kappa_{\max} \\ 0 & \text{otherwise.} \end{cases} \qquad [4]$$

(For mutualistic networks, another relevant parameter that is vulnerable to environmental change is the mutualistic interaction strength. The pertinent results are presented in *SI Appendix*.) To calculate the probability of R-tipping, $\Phi(r)$, we set $r = 0$ so that $\kappa = \kappa_{\min}$, solve Eqs. **3a** and **3b** numerically for a large number of random initial conditions chosen uniformly from the whole high-dimensional phase space, and determine 10^5 initial conditions that approach the high stable steady state in which no species becomes extinct. We then increase the rate r from zero. For each fixed value of r, we calculate, for each of the selected 10^5 initial conditions, whether or not the final state is the high stable state. If yes, then there is no R-tipping for the particular initial condition. However, if the final state becomes the extinction state, R-tipping has occurred for this value of r. The probability $\Phi(r)$ can be approximated by the fraction of the number of initial conditions leading to R-tipping out of the 10^5 initial conditions.

Fig. 1 shows $\Phi(r)$ versus r for the ten empirical mutualistic networks specified in Table 1, together with the bipartite network structure, which are distinguished by different colors. For each network, the interval $[\kappa_{\min}, \kappa_{\max}]$ of the bifurcation parameter (listed in the fifth column of Table 1) is chosen such that the dynamical network for static parameter values exhibits two stable steady states and a tipping point in this interval, as determined by a computational bifurcation analysis of the species abundances versus κ. Despite the differences in the topology and the specific parameter values among the empirical networks, it is remarkable that the probability of R-tipping exhibits a characteristic behavior common among all the networks: As the time-varying rate of the bifurcation parameter increases from zero, the probability increases rapidly and then saturates at an approximately finite constant value, as quantified by the analytic scaling law Eq. **1**. The final or asymptotic value of the R-tipping probability attained in the regime of large time rate of change of the bifurcation parameter depends on the specifics of the underlying mutualistic network in terms of its topological structure and basic system parameters. For example, the total number of species, or the phase-space dimension of the underlying dynamical system, and the relative numbers of the pollinator and plant species vary dramatically across the ten networks, as indicated by the ten surrounding network-structure diagrams in Fig. 1. The structural and parametric disparities among the networks lead to different relative basin volumes of the survival and extinction stable steady states, giving rise to distinct asymptotic probabilities of R-tipping.

The ecological interpretation of the observed different asymptotic values of the R-tipping probability is as follows. Previous studies revealed the complex interplay between the structural properties of the network and environmental factors in shaping

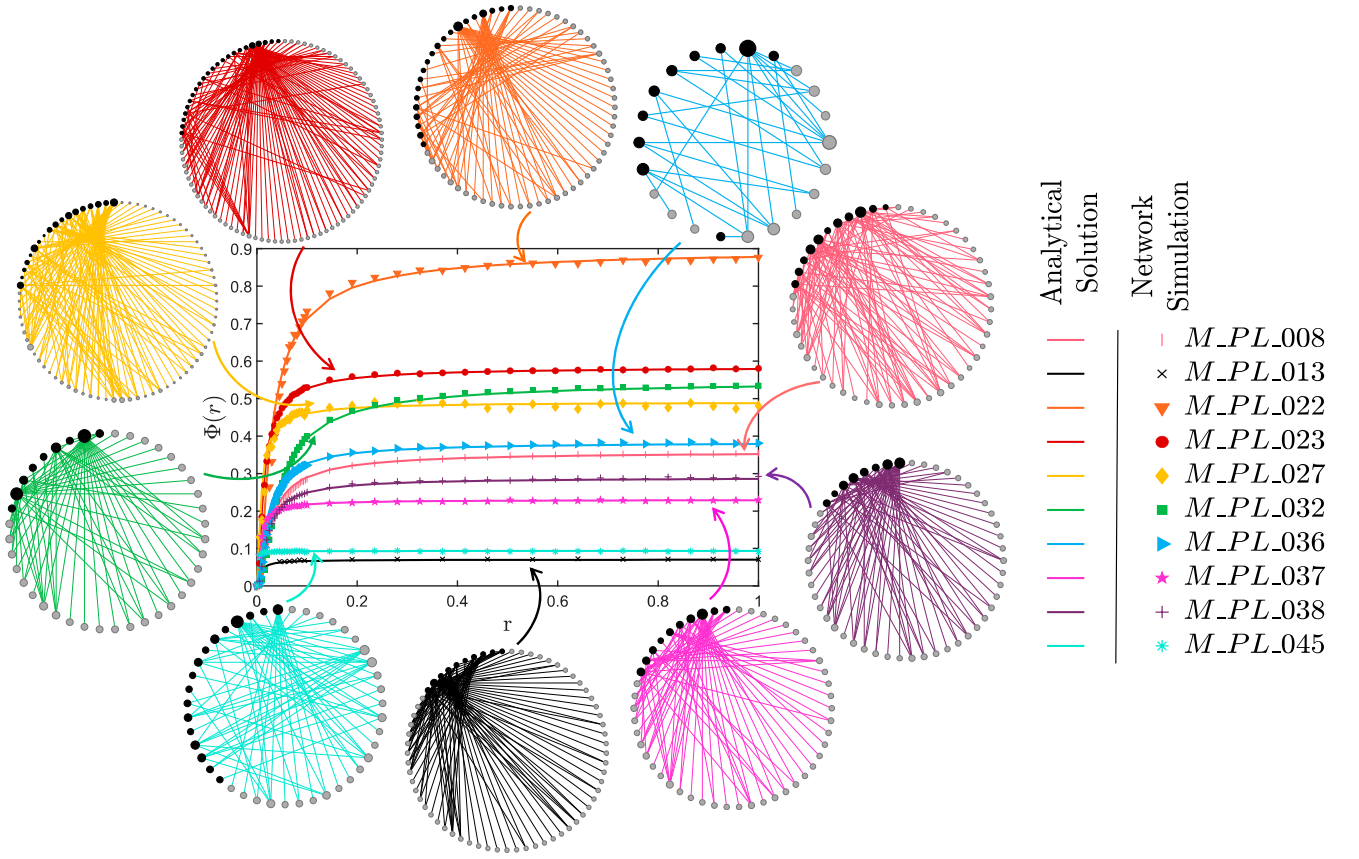

Fig. 1. Probability $\Phi(r)$ of R-tipping versus the time rate r of parameter change for ten real-world mutualistic networks, together with the corresponding bipartite structure for each network. The dots are the probability calculated by simulating Eqs. **3a**, **3b**, and **4**, with an ensemble of random initial conditions. The solid curves are the analytic results from Eq. **1**, with the two fitting parameters B and C given in Table 1. Other parameter values are $\alpha = 0.3$, $\beta = 1$, $h = 0.4$, $\gamma^P = 1.93$, and $\gamma^A = 1.77$.

extinction probabilities (53–60). For example, it was discovered (53) that the plant species tend to play a more significant role in the health of the network system as compared to pollinators (53) in the sense that plant extinction due to climate change is more likely to trigger pollinator coextinction than the other way around. In another example, distinct topological features were found to be associated with the networks with a higher probability of extinction (54, 55). It was also found that robust plant–pollinator mutualistic networks tend to exhibit a combination of compartmentalized and nested patterns (55). More generally, mutualistic networks in the real world are quite diverse in their structure and parameters, each possessing one or two or all the features including lower interaction density, heightened specialization, fewer pollinator visitors per plant species, lower nestedness, and lower modularity, etc. (54–60). It is thus reasonable to hypothesize that the asymptotic value of the R-tipping probability can be attributed to the sensitivity of the underlying network to environmental changes. For example, a higher (lower) saturation value of the extinction probability can be associated with the networks with a large (small) number of plants and lower (higher) nestedness, network *M_PL_22* (network *M_PL_13*). In other examples, network *M_PL_32* can be categorized as "vulnerable" due to its low modularity, despite having a small number of plants, and network *M_PL_45* is resilient against extinction due to its high nestedness and high modularity.

The remarkable phenomenon is that, in spite of these differences, the rapid initial increase in the R-tipping probability is shared by all ten networks! That is, when a parameter begins to change with time from zero, even slowly, the probability of R-tipping increases dramatically. The practical implication is that ecosystems with time-dependent parameter drift are highly susceptible to R-tipping. Parameter drifting, even at a slow pace, will be detrimental. This poses a daunting challenge to preserving ecosystems against negative environmental changes. In particular, according to conventional wisdom, ecosystems can be effectively protected by slowing down the environmental changes, but our results suggest that catastrophic tipping can occur with a finite probability unless the rate of the environmental changes is reduced to a near zero value.

To further explore the effects of parameter changes, we study a scenario in which negative environmental impacts cause the species decay rate (κ) and the mutualistic interaction strength (γ_0) to linearly increase and decrease, respectively. By considering the rate of changing of κ (γ_0) as r_κ (r_{γ_0}), we set $r_\kappa = \mathcal{C} r_{\gamma_0}$, which allows us to investigate three different scenarios by varying the parameter $\mathcal{C}$: $\mathcal{C} < 1$, $\mathcal{C} = 1$, and $\mathcal{C} > 1$. Fig. 2 shows a systematic analysis of the tipping-point transitions in the 2D parameter plane along with the probability of R-tipping for the three different scenarios for the network M_PL_032. (The pertinent results for the other nine networks are presented in *SI Appendix*, section 4.)

To understand the behavior of the R-tipping probability in Fig. 1, we resort to the approach of dimension reduction (61). In particular, for tipping-point dynamics, a high-dimensional mutualistic network can be approximated by an effective model of two dynamical variables: the respective mean abundances of

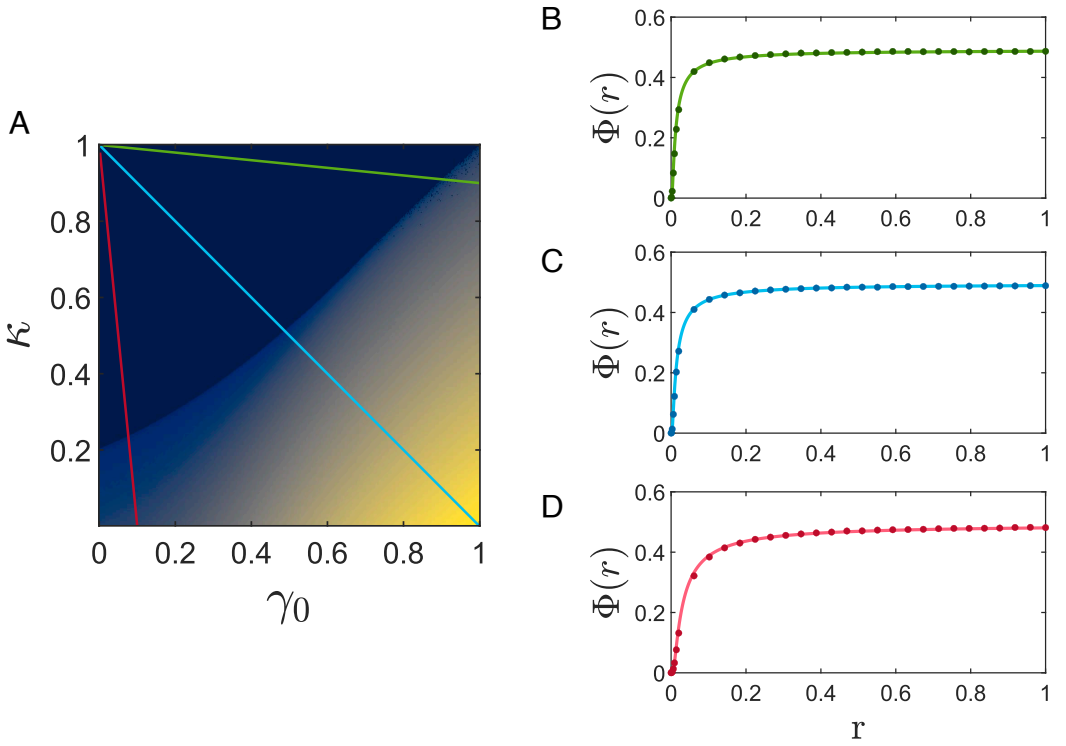

Fig. 2. Scaling law of probability of R-tipping in 2D parameter space. (*A*) 2D parameter plane of the species decay rate (κ) and the mutualistic interaction strength (γ_0) for the network M_PL_032. The solid lines correspond to the three different scenarios of the parameter $\mathcal{C}$ in calculating the probability of the R-tipping point from 10^7 initial conditions for (*B*) $\mathcal{C} < 1$, (*C*) $\mathcal{C} = 1$, and (*D*) $\mathcal{C} > 1$. Other parameters are $t = 0.5$, $\beta = 1$, $\alpha = 0.3$, and $h = 0.4$.

all pollinator and plant species. The effective 2D model can be written as ref. 17

$$\dot{P} = P\Big(\alpha - \beta P + \frac{\gamma^P A}{1 + h\gamma^P A}\Big), \qquad [5a]$$

$$\dot{A} = A\Big(\alpha - \kappa - \beta A + \frac{\gamma^A P}{1 + h\gamma^A P}\Big), \qquad [5b]$$

where P and A are the average abundances of all the plants and pollinators, respectively, α is the effective growth rate, and parameter β characterizes the combined effects of intraspecific and interspecific competition. The parameters γ^P and γ^A are the effective mutualistic interaction strengths that can be determined by the method of eigenvector weighting (17) (*SI Appendix*, Note 1). Eqs. **5a** and **5b** possess five possible equilibria: $\mathbf{f}_1 \equiv (0, 0)^T$, $\mathbf{f}_2 \equiv (\alpha/\beta, 0)^T$, $\mathbf{f}_3 \equiv (0, (\alpha - \kappa)/\beta)^T$, and $\mathbf{f}_{4,5} \equiv (g_1, g_2)^T$, where g_1 and g_2 are two possible equilibria that depend on the values of the parameters of the model and can be calculated by setting zero the factor in the parentheses of Eqs. **5a** and **5b**.

The first equilibrium $\mathbf{f}_1$, an extinction state, is at the origin $(P^*, A^*) = (0, 0)$ and is unstable. The second equilibrium $\mathbf{f}_2$ is located at the $(P^*, A^*) = (\alpha/\beta, 0)$ and it can be stable or unstable depending on the parameters κ. The locations of the remaining equilibria depend on the value of κ. In particular, the third equilibrium $\mathbf{f}_3$ can be unstable or nonexistent and the fourth equilibrium $\mathbf{f}_4$ is stable and coexists with stable equilibrium $\mathbf{f}_2$ in some interval of κ. The fifth equilibrium $\mathbf{f}_5$ is an unstable saddle fixed point in some relevant interval of κ. Fig. 3 *A* and *B* exemplify the behaviors of the equilibria as κ increases from zero to one for $\alpha = 0.3$, $\beta = 1$, $h = 0.4$, $\gamma^P = 1.93$, and $\gamma^A = 1.77$, for the average plant and pollinator abundances, respectively. In each panel, the upper green curve is the survival fixed point $\mathbf{f}_4$, while the lower horizontal green line corresponds to the extinction state $\mathbf{f}_2$. The blue dot-dashed ellipse indicates the interval of κ in which two stable equilibria coexist (bistability), whose right edge marks a tipping point.

What will happen to the dynamics when the parameter κ becomes time dependent? Without loss of generality, we focus on the interval of κ as exemplified by the horizontal range of the dot-dashed ellipse in Fig. 3 *A* and *B*, defined as $[\kappa_{\min}, \kappa_{\max}]$, in which there is bistability in the original high-dimensional network and in the 2D reduced model as well. Note that, for different high-dimensional empirical networks, the values of $\kappa_{\min}$ and $\kappa_{\max}$ in the 2D effective models are different, as illustrated in the fifth column of Table 1. Because of the coexistence of two stable fixed points, for every parameter value in the range $[\kappa_{\min}, \kappa_{\max}]$, there are two basins of attraction, as illustrated in Fig. 3 *C* and *D* for the 2D effective model of an empirical network M_PL_036 for $\kappa = 0.74$ and $\kappa = 0.88$, respectively, where the pink and gray regions correspond to the basins of the extinction and survival attractors, respectively. The basin boundary is the stable manifold of the unstable fixed point $\mathbf{f}_5$. It can be seen that, as κ increases, the basin of the extinction attractor increases, accompanied by a simultaneous decrease in the basin area of the survival attractor. This can be understood by comparing the positions of the equilibria in Fig. 3 where, as κ increases, the position of survival fixed point $\mathbf{f}_4$ moves toward lower plant and pollinator abundances, but the unstable fixed point $\mathbf{f}_5$ moves in the opposite direction: the direction of larger species abundances.

The boundary separating the basins of the extinction and survival fixed-point attractors is the stable manifold of $\mathbf{f}_5$. As r increases from zero, $\mathbf{f}_5$ moves in the direction of larger plant and pollinator abundances, so must the basin boundary, as exemplified in Fig. 4 (the various dashed curves) for $r \in [0, 1]$.

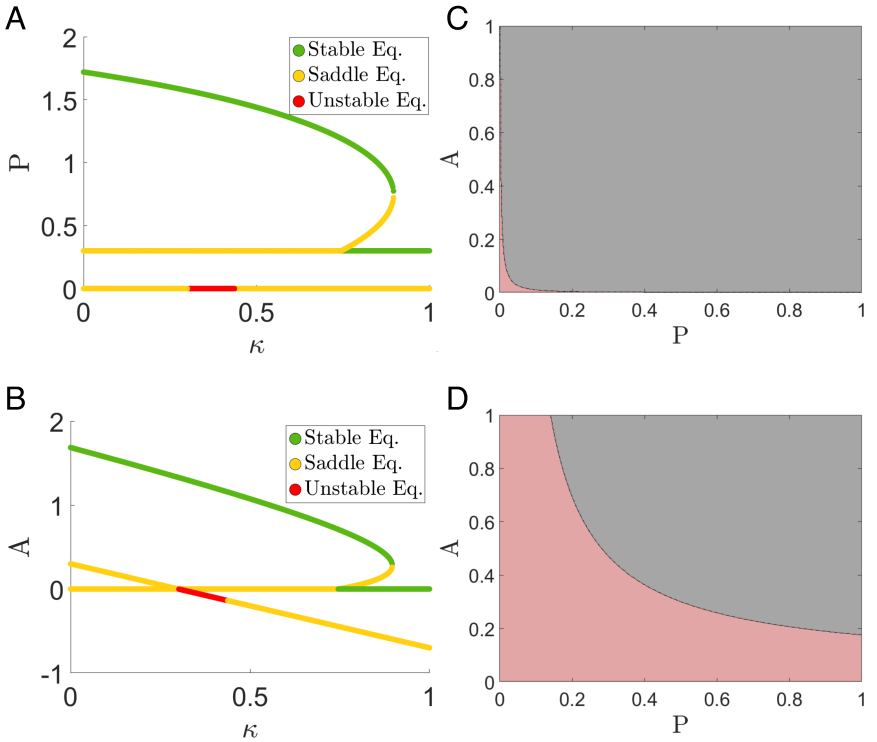

Fig. 3. Dynamics of the 2D reduced model Eqs. **5a** and **5b**. (*A* and *B*) A tipping point occurs as the species decay rate κ increases toward one, for the mean plant and pollinator abundances, respectively. The green and yellow curves correspond to the stable and unstable steady states, respectively, where the yellow curve with a red segment is the unstable fixed point $\mathbf{f}_5$. The region of bistability is indicated by the blue dot-dashed ellipses. (*C* and *D*) Examples of basins of attraction of the 2D model whose parameters are determined as the corresponding averages from the empirical network M_PL_036 in Table 1 for $\kappa_{\min} = 0.74$ and $\kappa_{\max} = 0.88$, respectively. Other parameters are $\alpha = 0.3$, $\beta = 1$, $h = 0.4$, $\gamma^P = 1.93$, and $\gamma^A = 1.77$. The pink and gray regions correspond to the basins of the stable steady states f_2 (extinction) and f_4 (survival), respectively.

Note that, since the decay parameter κ increases from $\kappa_{\min}$ to $\kappa_{\max}$ at the linear rate r, we have $\kappa(r = 0) = \kappa_{\min}$ and $\kappa(r = \infty) = \kappa_{\max}$. As r increases, the basin boundaries accumulate at the one for $\kappa_{\max}$.

Theory

Fig. 4 provides a physical base for deriving the scaling law Eq. **1**. Consider the small neighborhood of the unstable fixed point $\mathbf{f}_5$, where the basin boundary is approximately straight, as shown schematically in Fig. 5. Consider two cases: one with rate r_1 of parameter increase and another with rate r_2, where $r_2 > r_1$, as shown in Fig. 5 *A* and *B*, respectively. For any given rate r, at the beginning and end of the parameter variation, we have $\kappa = \kappa_{\min}$ and $\kappa = \kappa_{\max}$, respectively, where the time it takes to complete this process is $T = (\kappa_{\max} - \kappa_{\min})/r$. Since $r_2 > r_1$, we have $T_2 < T_1$. For both Fig. 5 *A* and *B*, the unstable fixed point $\mathbf{f}_5$ is marked by the filled green circles at $t = 0$ and filled orange circles at the end of the parameter variation, and the blue dashed line with an arrow indicates the direction of change in the location of $\mathbf{f}_5$ in the phase space as the parameter varies with time. Likewise, the solid green (orange) line segments through $\mathbf{f}_5$ denote the boundary separating the extinction basin from the survival basin of attraction at $t = 0$ ($t = T_1$ or T_2). That is, before the parameter variation is turned on for $\kappa = \kappa_{\min}$, the initial conditions below (above) the solid green lines belong to the basin of the extinction (survival) attractor. After the process of parameter variation ends so that $\kappa = \kappa_{\max}$, the initial conditions below (above) the solid orange lines belong to the basin of the extinction (survival) attractor. During the process of parameter variation, $\mathbf{f}_5$ moves from the position of the green circle to that of the orange circle, and its stable manifold (the basin boundary) moves accordingly. Now consider the initial conditions in the light-shaded green area, which belong to the basin of the survival attractor for $\kappa = \kappa_{\min}$. Without parameter variation, as time goes, this green rectangular area will be stretched along the unstable direction of $\mathbf{f}_5$ exponentially according to its unstable eigenvalue λ and compressed exponentially in the stable direction, evolving into an orange rectangle that is long in the unstable direction. Since $T_1 > T_2$, the orange rectangle for $r = r_1$ is longer and thinner than that for $r = r_2$.

The dynamical mechanism responsible for R-tipping can now be understood based on the schematic illustration in Fig. 5 *A* and *B*. In particular, because of the movement of $\mathbf{f}_5$ and the basin boundary as the parameter variation is turned on, the dark shaded orange part of the long rectangle now belongs to the basin of the extinction attractor. The initial conditions in the original green rectangle which evolve into this dark-shaded orange region are nothing but the initial conditions that switch their destinations from the survival to the extinction attractor as the result of the time variation of the parameter. That is, these initial conditions will experience R-tipping, as indicated by the red rectangle inside the green area in Fig. 5*B*. For any given rate r, the fraction of such initial conditions determines the R-tipping probability. Let $d(0)$ denote the fraction of R-tipping initial conditions and let D be the distance between the basin boundaries at the beginning and end of parameter variation along the unstable direction of $\mathbf{f}_5$. We have $d(T) = D = d(0)\exp(\lambda T)$. Our argument for $\Phi(r) \sim d(0)$ and the use of $T = (\kappa_{\max} - \kappa_{\min})/r$ lead to the scaling law Eq. **1**.

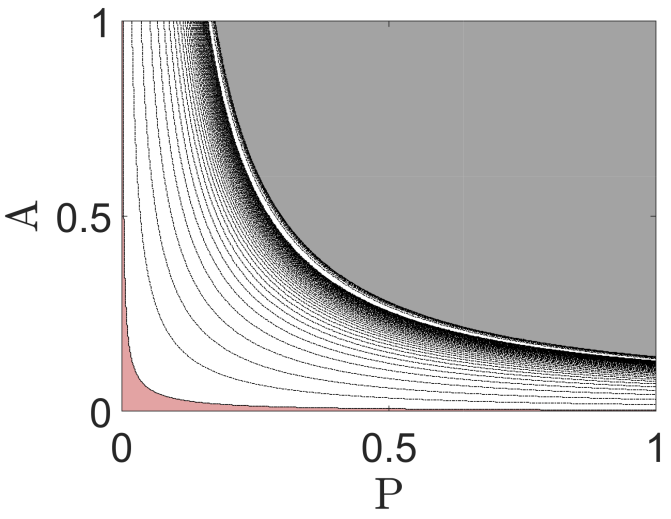

Fig. 4. Basin boundary between the extinction and survival fixed-point attractors for different rate of parameter change. Shown are a series of basin boundaries for $r \in [0\,1]$. As r increases from zero, the boundary moves in the direction of large species abundances. The basin boundaries are calculated from the 2D model of the empirical network M_PL_036 in Table 1. Other parameters are the same as those in Fig. 3 *C* and *D*.

Discussion

To summarize, nonlinear dynamical systems in nature such as ecosystems and climate systems on different scales are experiencing parameter changes due to increasing human activities, and it is of interest to understand how the "pace" or rate of parameter change might lead to catastrophic consequences. To this end, we studied high-dimensional mutualistic networks, as motivated by the following general considerations. In ecosystems, mutualistic interactions, broadly defined as a close, interdependent, mutually beneficial relationship between two species, are one of the most fundamental interspecific relationships. Mutualistic networks contribute to biodiversity and ecosystem stability. As species within these networks rely on each other for essential services, such as pollination, seed dispersal, or nutrient exchange, they promote species coexistence and reduce competitive exclusion. This coexistence enhances the overall diversity of the ecosystem, making it more resilient to disturbances and less susceptible to the dominance of a few species. They can drive coevolutionary processes between interacting species. As species interact over time, they may evolve in response to each other's adaptations, leading to reciprocal changes that strengthen the mutualistic relationship. Disruptions to these networks, such as the decline of pollinator populations, can have cascading effects on ecosystem functions and the survival of dependent species. By studying mutualistic interactions, conservationists can design more effective strategies to protect and restore these vital relationships and the ecosystems they support.

This paper focuses on the phenomenon of rate-induced tipping or R-tipping, where the rate of parameter change can cause the system to experience a tipping point from normal functioning to collapse. The main accomplishments are three. First, we went beyond the existing local approaches to R-tipping by taking a global approach of dynamical analysis based on consideration of basins of attraction of coexisting attractors. This allows us to introduce the probability of R-tipping with respect to initial conditions taken from the whole phase space. Second, most previous works on R-tipping analyzed low-dimensional toy models but our study focused on high-dimensional mutualistic networks constructed from empirical data. Third, we developed

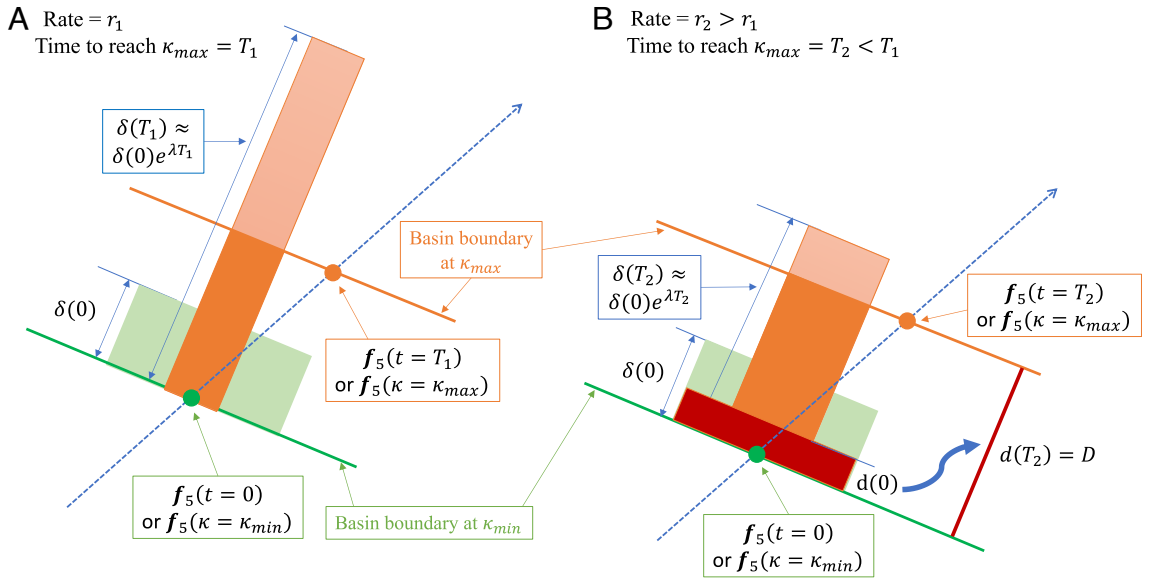

Fig. 5. Analysis of the dynamical mechanism responsible for R-tipping. The dynamics of the unstable fixed point $\mathbf{f}_5$ together with those of a rectangle region of the initial conditions in its neighborhood are illustrated for two values of the rate of parameter change: (*A*) $r = r_1$ and (*B*) $r = r_2 > r_1$. At $t = 0$ ($\kappa = \kappa_{\min}$, a segment of the basin boundary in the vicinity of $\mathbf{f}_5$ is illustrated as the solid green line. As the rate of parameter change begins to increase, the basin boundary moves upward and eventually accumulates at that for $\kappa = \kappa_{\max}$—the solid orange lines. For a small rate, the time required for the green boundary to reach the orange boundary is longer. All the initial conditions in the light green region above the green boundary belong to the basin of the survival attractor for $\kappa = \kappa_{\min}$, whose trajectories are determined by the local exponentially contracting and expanding dynamics of $\mathbf{f}_5$. The fate of these initial conditions is the result of a "race" to go above the orange basin boundary within the "allowed" time duration [T_1 in (*A*) and $T_2 < T_1$ in (*B*)]: Those managing to go above will approach the survival attractor, but those that stay below will lead to extinction. Since $T_1 > T_2$, the fraction of initial conditions that can go above in (*A*) is larger than that in (*B*), leading to a higher probability of R-tipping for case (*B*). The precise fraction of those initial conditions is indicated by the red rectangular region in (*B*), whose initial height stretches to the distance between the green and orange boundaries in the permissible time. This gives the probability of R-tipping as quantified by the scaling law Eq. **1**. See text for more details.

a geometric analysis and derived a scaling law governing the probability of R-tipping with respect to the rate of parameter change. The scaling law contains two parameters which, for two-dimensional systems, can be determined theoretically from the dynamics. For high-dimensional systems, the two scaling parameters can be determined through numerical fitting. For all ten empirical networks studied, the scaling law agrees well with the results from direct numerical simulations. To our knowledge, no such quantitative law characterizing R-tipping has been uncovered previously.

The effective 2D systems in our study were previously derived (17), which capture the bipartite and mutualistic nature of the ecological interactions in the empirical, high-dimensional networks. It employs one collective variable to account for the dynamical behavior of the pollinators and another for the plants. The effective 2D models allow us to mathematically analyze the global R-tipping dynamics, with results and the scaling law verified by direct simulations of high-dimensional networks. The key reason that the dimension-reduced 2D models can be effective lies, again, in the general setting of the ecological systems under consideration: coexistence of a survival and an extinction state. While our present work focused on mutualistic networks, we expect the global approach to R-tipping and the scaling law to be generally applicable to ecological systems in which large-scale extinction from a survival state is possible due to even a small, nonzero rate of parameter change.

It is worth noting that the setting under which the scaling law of the probability of R-tipping with the rate of parameter change holds is the coexistence of two stable steady states in the phase space, one associated with survival and another corresponding to extinction. This setting is general for studying tipping, system collapse, and massive extinction in ecological systems. Our theoretical analysis leading to the scaling law requires minimal conditions: two coexisting basins of attraction separated by a basin boundary. The scaling law is not the result of some specific parameterization of the mutualistic systems but is a generic feature in systems with two coexisting states. Insofar as the system can potentially undergo a transition from the survival to the extinction state, we expect our R-tipping scaling law to hold. In a broad context, coexisting stable steady states or attractors are ubiquitous in nonlinear physical and biological systems.

The scaling law stipulates that, as the rate increases from zero, the R-tipping probability increases rapidly first and then saturates. This has a striking and potentially devastating consequence: in order to reduce the probability of R-tipping, the parameter change must be slowed down to such an extent that its rate of change is practically zero. This has serious implications. For example, to avoid climate-change-induced species extinction, it would be necessary to ensure that no parameters change with time, and this may pose an extremely significant challenge in our efforts to protect and preserve the natural environment.

Data, Materials, and Software Availability. All study data are included in the article and/or *SI Appendix*.

ACKNOWLEDGMENTS. We thank Prof. Karen Abbott, Prof. Kim Cuddington, Dr. Christopher M. Heggerud, Dr. Andrey Morozov, Prof. Sergei Petrovskiy, and Prof. Mary Lou Zeeman for stimulating discussions. This work was supported by the Air Force Office of Scientific Research under Grant No. FA9550-21-1-0438. Y.D. was supported by the National Research Foundation of Korea grant funded by the Korean government Ministry of Science and Information and Communication Technology (MSIT) (Nos. NRF-2022R1A5A1033624 and 2022R1A2C3011711).

Author affiliations: [a]School of Electrical, Computer and Energy Engineering, Arizona State University, Tempe, AZ 85287; [b]Department of Mathematics, Nonlinear Dynamics Mathematical Application Center, Kyungpook National University, Daegu 41566, Republic of Korea; [c]Department of Environmental Science and Policy, University of California, Davis, CA 95616; [d]Santa Fe Institute, Santa Fe, NM 87501; and [e]Department of Physics, Arizona State University, Tempe, AZ 85287

1. M. Scheffer, *Ecology of Shallow Lakes* (Springer Science & Business Media, 2004).
2. M. Scheffer *et al*., Early-warning signals for critical transitions. *Nature* **461**, 53–59 (2009).
3. M. Scheffer, Complex systems: Foreseeing tipping points. *Nature* **467**, 411–412 (2010).
4. D. B. Wysham, A. Hastings, Regime shifts in ecological systems can occur with no warning. *Ecol. Lett.* **13**, 464–472 (2010).
5. J. M. Drake, B. D. Griffen, Early warning signals of extinction in deteriorating environments. *Nature* **467**, 456–459 (2010).
6. L. Chen, R. Liu, Z.-P. Liu, M. Li, K. Aihara, Detecting early-warning signals for sudden deterioration of complex diseases by dynamical network biomarkers. *Sci. Rep.* **2**, 342 (2012).
7. C. Boettiger, A. Hastings, Quantifying limits to detection of early warning for critical transitions. *J. R. Soc. Interface* **9**, 2527–2539 (2012).
8. L. Dai, D. Vorselen, K. S. Korolev, J. Gore, Generic indicators for loss of resilience before a tipping point leading to population collapse. *Science* **336**, 1175–1177 (2012).
9. P. Ashwin, S. Wieczorek, R. Vitolo, P. Cox, Tipping points in open systems: Bifurcation, noise-induced and rate-dependent examples in the climate system. *Phil. Trans. R. Soc. A Math. Phys. Eng. Sci.* **370**, 1166–1184 (2012).
10. T. M. Lenton, V. N. Livina, V. Dakos, E. H. van Nes, M. Scheffer, Early warning of climate tipping points from critical slowing down: Comparing methods to improve robustness. *Phil. Trans. Roy. Soc. A* **370**, 1185–1204 (2012).
11. A. D. Barnosky *et al*., Approaching a state shift in earth's biosphere. *Nature* **486**, 52–58 (2012).
12. C. Boettiger, A. Hastings, Tipping points: From patterns to predictions. *Nature* **493**, 157–158 (2013).
13. J. M. Tylianakis, C. Coux, Tipping points in ecological networks. *Trends Plant Sci.* **19**, 281–283 (2014).
14. J. Jelle Lever, E. H. Nes, M. Scheffer, J. Bascompte, The sudden collapse of pollinator communities. *Ecol. Lett.* **17**, 350–359 (2014).
15. T. S. Lontzek, Y.-Y. Cai, K. L. Judd, T. M. Lenton, Stochastic integrated assessment of climate tipping points indicates the need for strict climate policy. *Nat. Clim. Change* **5**, 441–444 (2015).
16. S. Gualdia, M. Tarziaa, F. Zamponic, J.-P. Bouchaudd, Tipping points in macroeconomic agent-based models. *J. Econ. Dyn. Contr.* **50**, 29–61 (2015).
17. J. Jiang *et al*., Predicting tipping points in mutualistic networks through dimension reduction. *Proc. Natl. Acad. Sci. U.S.A.* **115**, E639–E647 (2018).
18. B. Yang *et al*., Dynamic network biomarker indicates pulmonary metastasis at the tipping point of hepatocellular carcinoma. *Nat. Commun.* **9**, 678 (2018).
19. J. Jiang, A. Hastings, Y.-C. Lai, Harnessing tipping points in complex ecological networks. *J. R. Soc. Interface* **16**, 20190345 (2019).
20. M. Scheffer, *Critical Transitions in Nature and Society* (Princeton University Press, 2020), vol. 16.
21. Yu. Meng, J. Jiang, C. Grebogi, Y.-C. Lai, Noise-enabled species recovery in the aftermath of a tipping point. *Phys. Rev. E* **101**, 012206 (2020).
22. Yu. Meng, Y.-C. Lai, C. Grebogi, Tipping point and noise-induced transients in ecological networks. *J. R. Soc. Interface* **17**, 20200645 (2020).
23. Yu. Meng, C. Grebogi, Control of tipping points in stochastic mutualistic complex networks. *Chaos* **31**, 023118 (2021).
24. Yu. Meng, Y.-C. Lai, C. Grebogi, The fundamental benefits of multiplexity in ecological networks. *J. R. Soc. Interface* **19**, 20220438 (2022).
25. P. E. O'Keeffe, S. Wieczorek, Tipping phenomena and points of no return in ecosystems: Beyond classical bifurcations. *SIAM J. Appl. Dyn. Syst.* **19**, 2371–2402 (2020).
26. C. Trefois, P. M. A. Antony, J. Goncalves, A. Skupin, R. Balling, Critical transitions in chronic disease: Transferring concepts from ecology to systems medicine. *Cur. Opin. Biotechnol.* **34**, 48–55 (2015).
27. K. Albrich, W. Rammer, R. Seidl, Climate change causes critical transitions and irreversible alterations of mountain forests. *Global Change Biol.* **26**, 4013–4027 (2020).
28. A. Bayani, F. Hadaeghi, S. Jafari, G. Murray, Critical slowing down as an early warning of transitions in episodes of bipolar disorder: A simulation study based on a computational model of circadian activity rhythms. *Chronobiol. Int.* **34**, 235–245 (2017).
29. A. D. Synodinos *et al*., The rate of environmental change as an important driver across scales in ecology. *Oikos* **2023**, e09616 (2022).
30. J. T. Morris, P. V. Sundareshwar, C. T. Nietch, B. Kjerfve, D. R. Cahoon, Responses of coastal wetlands to rising sea level. *Ecology* **83**, 2869–2877 (2002).
31. P. D. L. Ritchie, H. Alkhayuon, P. M. Cox, S. Wieczorek, Rate-induced tipping in natural and human systems. *Earth Syst. Dyn.* **14**, 669–683 (2023).
32. S. Wieczorek, P. Ashwin, C. M. Luke, P. M. Cox, Excitability in ramped systems: The compost-bomb instability. *Proc. R. Soc. A Math. Phys. Eng. Sci.* **467**, 1243–1269 (2011).
33. J. Mitry, M. McCarthy, N. Kopell, M. Wechselberger, Excitable neurons, firing threshold manifolds and canards. *J. Math. Neurosci.* **3**, 1–32 (2013).
34. N. A. Alexander, O. Oddbjornsson, C. A. Taylor, H. M. Osinga, D. E. Kelly, Exploring the dynamics of a class of post-tensioned, moment resisting frames. *J. Sound Vib.* **330**, 3710–3728 (2011).
35. S.-Y. Hsu, M.-H. Shih, The tendency toward a moving equilibrium. *SIAM J. Appl. Dyn. Sys.* **14**, 1699–1730 (2015).
36. P. Ashwin, C. Perryman, S. Wieczorek, Parameter shifts for nonautonomous systems in low dimension: Bifurcation-and rate-induced tipping. *Nonlinearity* **30**, 2185 (2017).
37. A. Vanselow, S. Wieczorek, U. Feudel, When very slow is too fast-collapse of a predator-prey system. *J. Theo. Biol.* **479**, 64–72 (2019).

38. R. Lande, S. Engen, B.-E. Saether, *Stochastic Population Dynamics in Ecology and Conservation* (Oxford University Press on Demand, 2003).
39. B. B. Hansen *et al*., More frequent extreme climate events stabilize reindeer population dynamics. *Nat. Commun.* **10**, 1616 (2019).
40. A. Hastings *et al*., Transient phenomena in ecology. *Science* **361**, eaat6412 (2018).
41. A. Morozov *et al*., Long transients in ecology: Theory and applications. *Phys. Life Rev.* **32**, 1–40 (2020).
42. J. Bascompte, P. Jordano, C. J. Melián, J. M. Olesen, The nested assembly of plant-animal mutualistic networks. *Proc. Natl. Acad. Sci. U.S.A.* **100**, 9383–9387 (2003).
43. P. R. Guimaraes, P. Jordano, J. N. Thompson, Evolution and coevolution in mutualistic networks. *Ecol. Lett.* **14**, 877–885 (2011).
44. S. L. Nuismer, P. Jordano, J. Bascompte, Coevolution and the architecture of mutualistic networks. *Evolution* **67**, 338–354 (2013).
45. R. P. Rohr, S. Saavedra, J. Bascompte, On the structural stability of mutualistic systems. *Science* **345**, 1253497 (2014).
46. V. Dakos, J. Bascompte, Critical slowing down as early warning for the onset of collapse in mutualistic communities. *Proc. Natl. Acad. Sci. U.S.A.* **111**, 17546–17551 (2014).
47. P. R. Guimaraes, M. M. Pires, P. Jordano, J. Bascompte, J. N. Thompson, Indirect effects drive coevolution in mutualistic networks. *Nature* **550**, 511–514 (2017).
48. T. Ohgushi, O. Schmitz, R. D. Holt, *Trait-Mediated Indirect Interactions: Ecological and Evolutionary Perspectives* (Cambridge University Press, Cambridge UK, 2012).
49. U. Bastolla *et al*., The architecture of mutualistic networks minimizes competition and increases biodiversity. *Nature* **458**, 1018–1020 (2009).
50. J. Bascompte, P. Jordano, Plant-animal mutualistic networks: The architecture of biodiversity. *Annu. Rev. Ecol. Evol. Syst.* **38**, 567–593 (2007).
51. P. J. Menck, J. Heitzig, N. Marwan, J. Kurths, How basin stability complements the linear-stability paradigm. *Nat. Phys.* **9**, 89–92 (2013).
52. C. S. Holling, Resilience and stability of ecological systems. *Annu. Rev. Ecol. Syst.* **4**, 1–23 (1973).
53. M. Schleuning *et al*., Ecological networks are more sensitive to plant than to animal extinction under climate change. *Nat. Commun.* **7**, 13965 (2016).
54. A. J. Vanbergen, B. A. Woodcock, M. S. Heard, D. S. Chapman, Network size, structure and mutualism dependence affect the propensity for plant-pollinator extinction cascades. *Funct. Ecol.* **31**, 1285–1293 (2017).
55. T. M. Lewinsohn, P. I. Prado, P. Jordano, J. Bascompte, J. M. Olesen, Structure in plant-animal interaction assemblages. *Oikos* **113**, 174–184 (2006).
56. D. P. Vázquez, N. Blüthgen, L. Cagnolo, N. P. Chacoff, Uniting pattern and process in plant-animal mutualistic networks: A review. *Ann. Bot.* **103**, 1445–1457 (2009).
57. C. E. Aslan, E. S. Zavaleta, B. Tershy, D. Croll, Mutualism disruption threatens global plant biodiversity: A systematic review. *PLoS One* **8**, e66993 (2013).
58. S. Sheykhali *et al*., Robustness to extinction and plasticity derived from mutualistic bipartite ecological networks. *Sci. Rep.* **10**, 9783 (2020).
59. M. M. Pires *et al*., The indirect paths to cascading effects of extinctions in mutualistic networks. *Ecology* **101** (2020).
60. J.-G. Young, F. S. Valdovinos, M. E. J. Newman, Reconstruction of plant-pollinator networks from observational data. *Nat. Commun.* **12**, 3911 (2021).
61. J. Gao, B. Barzel, A.-L. Barabási, Universal resilience patterns in complex networks. *Nature* **530**, 307–312 (2016).

PNAS

Supporting Information for

Rate-induced tipping in complex high-dimensional ecological networks

Shirin Panahi, Younghae Do, Alan Hastings, and Ying-Cheng Lai[1]

[1]To whom correspondence should be addressed. E-mail: Ying-Cheng.Lai@asu.edu

This PDF file includes:

Supporting text
Figs. S1 to S14
Tables S1 to S2
SI References

Supporting Information Text

1. Two-dimensional effective model

The reduced effective model of mutualistic networks described by Eq. 1 in the main text can be written as (1)

$$\dot{P} = P\Big(\alpha - \beta P + \frac{\gamma^P A}{1 + h\gamma^P A}\Big) \tag{1a}$$

$$\dot{A} = A\Big(\alpha - \kappa - \beta A + \frac{\gamma^A P}{1 + h\gamma^A P}\Big) \tag{1b}$$

where the dynamical variables P and A correspond to the average abundances of the plant and pollinator species, respectively, α is the effective growth rate, β is a parameter characterizing the combined effects of intraspecific and interspecific competition. To calculate the effective mutualistic interaction strengths γ^P and γ^A, we use the eigenvector weighting method (1). In particular, the pollinator and plant abundances are calculated based on the largest eigenvalue of the respective projection bipartite network where any direct interaction in the network is between a pollinator and a plant species. The projection matrix Ξ characterizing all mutualistic interactions is $N_P \times N_A$ dimensional, where N_P and N_A are the numbers of plant and pollinator species, respectively. For $\xi_{ij} = 1$, there is an interaction between the i^{th} plant and the j^{th} pollinator species; otherwise $\xi_{ij} = 0$. The project matrices Ξ_P and Ξ_A for the plan and pollinator species can be written as

$$\Xi_P = \Xi\Xi^T \quad \Xi_A = \Xi^T\Xi. \tag{2}$$

Let V_P and V_A be the eigenvectors associated with the largest eigenvalue of Ξ_P and Ξ_A, respectively. The effective mutualistic interaction strengths can be calculated through

$$\gamma^P = \frac{\gamma_0 \sum_{i=1}^{S_P} k_{P_i}^{1-t} V_P^i}{\sum_{i=1}^{S_P} V_P^i} \tag{3}$$

$$\gamma^A = \frac{\gamma_0 \sum_{i=1}^{S_A} k_{A_i}^{1-t} V_A^i}{\sum_{i=1}^{S_A} V_A^i} \tag{4}$$

Setting the right-hand side of Eqs. 1a and 1b to zero, we find five possible equilibria: $\mathbf{f}_1 \equiv (0,0)^T$, $\mathbf{f}_2 \equiv (\alpha/\beta, 0)^T$, $\mathbf{f}_3 \equiv (0, (\alpha-\kappa)/\beta)^T$, and $\mathbf{f}_{4,5} \equiv (g_1, g_2)^T$, where g_1 and g_2 are two possible equilibria that depend on the values of the model parameters and can be calculated by setting zero the factor in the parentheses of Eqs. 1a and 1b. The first equilibrium $\mathbf{f}_1$ is an unstable equilibrium corresponding to an extinction state located at the origin $(P^*, A^*) = (0,0)$. The second equilibrium $\mathbf{f}_2$ is located at the $(P^*, A^*) = (\alpha/\beta, 0)$, and its stability depends on the value of the parameters κ. The locations of all three remaining equilibria depend on the value of κ. In particular, the third equilibrium $\mathbf{f}_3 \equiv (0, (\alpha-\kappa)/\beta)^T$ is unstable for $\alpha > \kappa$ and does not exist for $\alpha < \kappa$ (corresponding to nonphysical negative abundances). The fourth equilibrium $\mathbf{f}_4$ is stable and it coexists with stable equilibrium $\mathbf{f}_2$. The fifth equilibrium $\mathbf{f}_5$ is an unstable saddle fixed point.

Figure S1 exemplifies the vector field, nullclines, and equilibria of the 2D effective model 1. For this parameter setting, the model exhibits bistability with two stable equilibria. The unstable saddle equilibria $\mathbf{f}_1$ and $\mathbf{f}_5$ are indicated by the yellow dots and stable equilibria $\mathbf{f}_2$ and $\mathbf{f}_4$ are denoted by the two green dots.

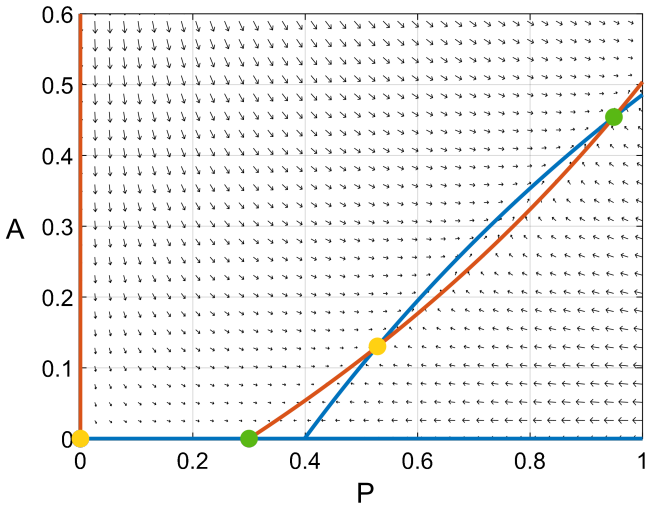

Fig. S1. Vector field of the reduced 2D system 1 for parameter values $\alpha = 0.3$, $\beta = 1$, $h = 0.4$, $\kappa = 0.85$, $\gamma^P = 1.93$, and $\gamma^\alpha = 1.77$. The blue and red curves are the nullclines of the pollinator and plant species, respectively. The yellow and green dots are the saddle and stable equilibria. The equilibrium $\mathbf{f}_3$ is located at $[0 - 0.55]$, which is nonphysical.

2. Probability of R-tipping in the effective model

As described in the main text, the probability of rate-induced tipping (or R-tipping) can be calculated for the 2D effective model that captures the essential tipping-point dynamics of the high-dimensional mutualistic network (1). As shown in Fig. 4 of the main text, as the time rate of change r of some parameter increases from zero, the basin boundary moves in the direction of larger plant and pollinator abundances. For $r = 0$ ($r = \infty$), the extinction basin (pink region) is the same as that in the $2D$ effective model 1 for $\kappa = \kappa_0$ ($\kappa = \kappa_{max}$). The greater the rate r, the larger the extinction area is.

To calculate the probability of R-tipping, $\Phi(r)$, we set $r = 0$ so that $\kappa = \kappa_{\min}$, solve Eqs. 1a and 1b for a large number of initial conditions chosen from the gray region of the phase space that approaches the high stable steady state in which no species is extinct. We then increase the rate r from zero. For each fixed value of r, we calculate, for each initial condition, whether the final state is the high stable state. If yes, then there is no R-tipping for the particular initial condition. However, if the final state becomes extinction, then R-tipping has occurred for this value of r. The probability $\Phi(r)$ can be approximated by the fraction of the number of initial conditions leading to R-tipping out of the whole chosen initial conditions.

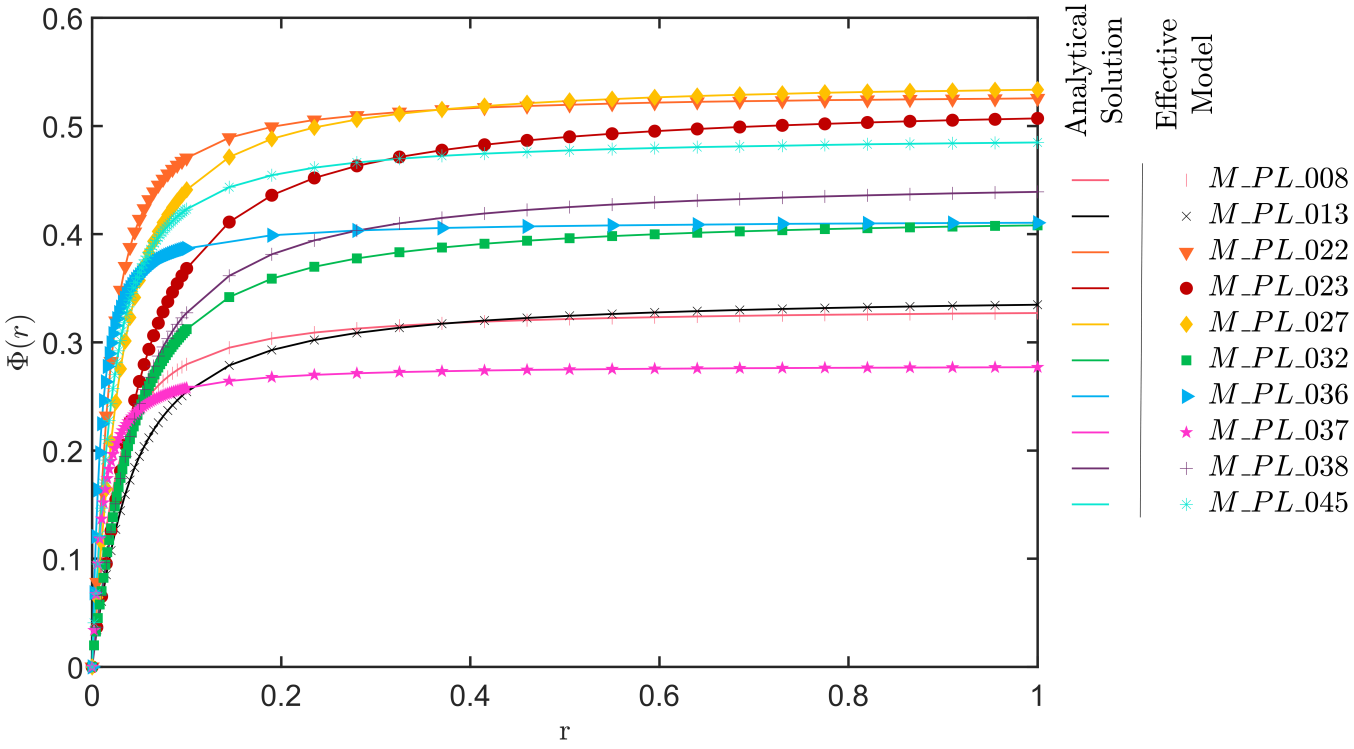

Fig. S2. Probability of R-tipping in the reduced 2D effective model versus the time rate of change of the pollinator decay parameter κ. For a given rate r, initially $\kappa = \kappa_{min}$ and it increases to κ_{max} at the rate r. Other parameters are fixed: $\alpha = 0.3$, $\beta = 1$, $h = 0.4$, $\gamma^P = 1.93$, $\gamma^A = 1.77$.

Figure S2 shows the probability of R-tipping $\Phi(r)$ in the 2D effective model versus the rate r for the cases corresponding to those in Table 1 in the main text. For each network, the range $[\kappa_{\min}, \kappa_{\max}]$ of parameter change is listed in the fifth column of Table 1 in the main text. The solid curves represent the analytic prediction. There is a good agreement between theory and numerics. The general feature is that, as the rate of parameter change increases from zero, the probability $\Phi(r)$ increases rapidly initially and then saturates at an approximately constant value, in agreement with the results from the high-dimensional networks in the main text.

3. Probability of R-tipping with time-varying mutualistic interaction γ_0

For a mutualistic network, the strength of the mutualistic interactions is another key parameter. Negative environmental impacts can cause the interactions to continuously weaken. This can be modeled by starting from an initial (relatively large) value of the nominal interaction strength γ_0^{max} and decreasing the parameter γ_0 at a constant rate until it reaches the minimum value γ_0^{min}, as shown in Fig. S3. The time required for the parameter change is $T = (\gamma_0^{min} - \gamma_0^{max})/r$, where $r < 0$.

As γ_0 decreases from its initial value, the unstable saddle point $\mathbf{f}_5$ starts to move from $\mathbf{f}_5(\gamma_0^{max})$ and reaches $\mathbf{f}_5(\gamma_0^{min})$ at time T. The trajectories starting from the initial conditions located above the stable manifold of $\mathbf{f}_5(\gamma_0^{max})$ leave exponentially from the unstable saddle point over time: $\sim e^{\lambda t}$. The number of initial conditions that are unable to catch up with the moving saddle point $\mathbf{f}_5(\gamma_0)$ is proportional to $e^{-\lambda T}$. The faster rate of change r, the larger the basin of extinction is. Using an argument similar to the one in the main text, we obtain

$$\Phi(r) = B \exp\left[-C\left(\frac{\gamma_0^{min} - \gamma_0^{max}}{r}\right)\right] \qquad [5]$$

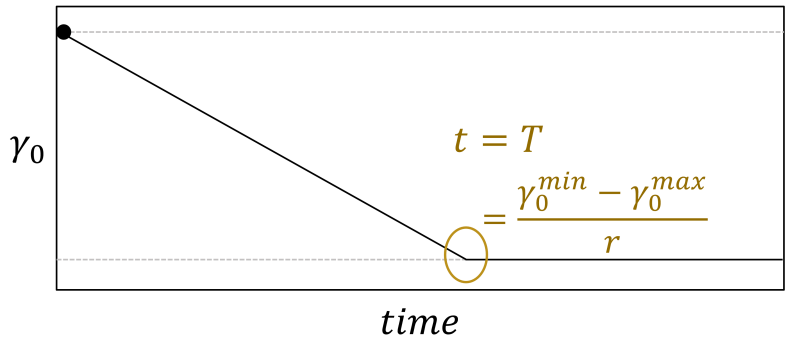

Fig. S3. Linear decrease in the nominal mutualistic interaction strength γ_0. The rate of decrease is r, the initial and final values of the strength are γ_0^{max}, and γ_0^{min}, respectively. The time required for the change is $T = (\gamma_0^{min} - \gamma_0^{max})/r$.

with $B > 0$ and $C > 0$ being two fitting constants. Fig. S4 shows the probability of R-tipping with respect to different values of rate r for all the networks listed in Table 1 in the main text. The details of the parameter setting and the values of the two fitting parameters for the ten high-dimensional mutualistic networks are provided in Table S1. As the rate of parameter change increases from zero, the probability of R-tipping increases rapidly initially and then saturates at an approximately constant value, similar to the cases treated in the main text where the time-varying parameter is the species decay rate.

Table S1. Empirical mutualistic networks, their ranges of parameter variations, and fitting constants in Eq. (5)

Network	κ	γ_0-interval	B	C
M_PL_008	0.92	[0.96 1]	0.05	0.12
M_PL_013	0.95	[0.95 1]	0.03	0.18
M_PL_022	0.89	[0.96 1]	0.39	0.04
M_PL_023	0.90	[0.92 1]	0.37	0.08
M_PL_027	0.93	[0.97 1]	0.11	0.07
M_PL_032	0.94	[0.94 1]	0.12	0.07
M_PL_036	0.8	[0.90 1]	0.10	0.11
M_PL_037	0.90	[0.97 1]	0.14	0.06
M_PL_038	0.93	[0.98 1]	0.23	0.05
M_PL_045	0.96	[0.98 1]	0.13	0.05

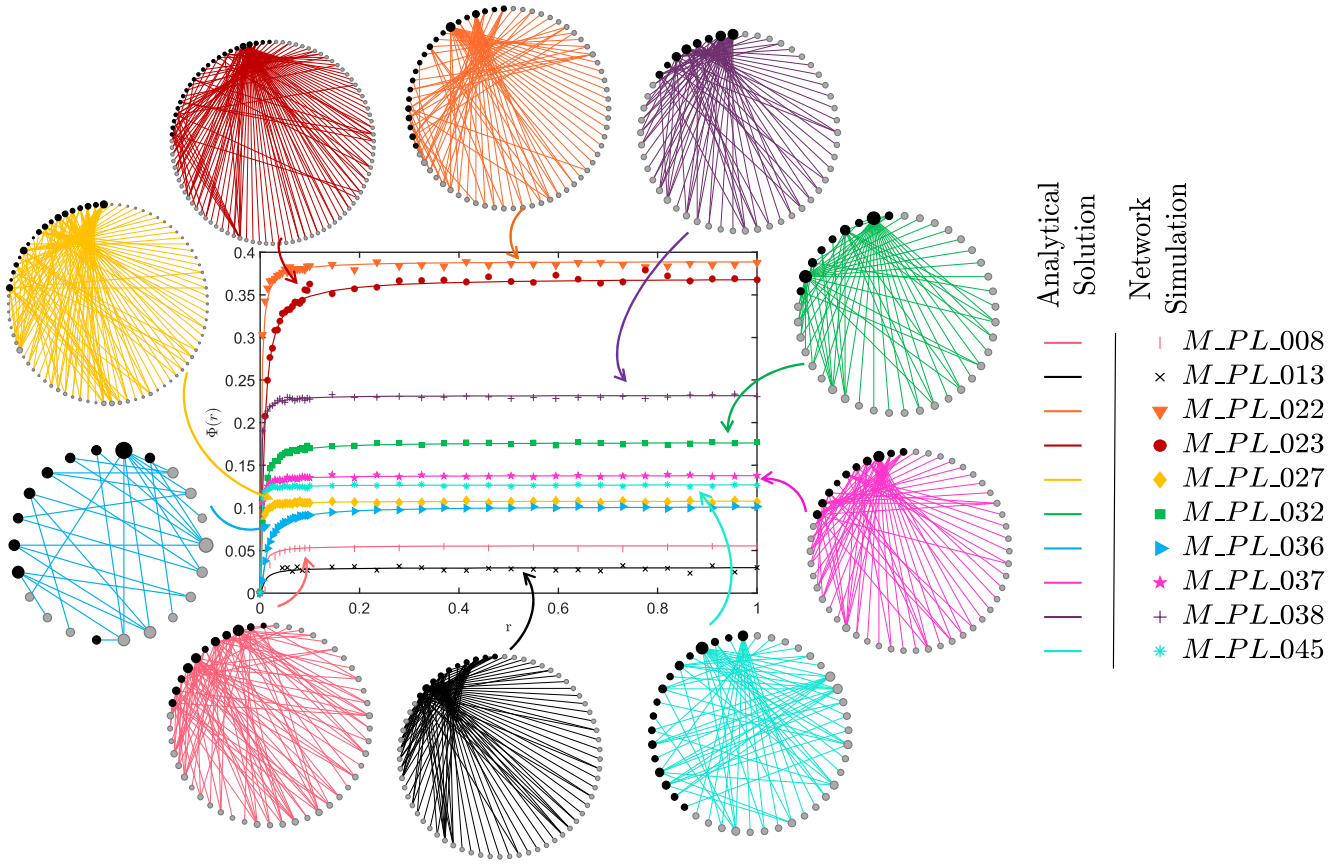

Fig. S4. Probability of the R-tipping versus the rate of change in the nominal mutualistic interaction strength. Initially, the strength is $\gamma_0 = \gamma_0^{max}$ and it linearly decreases to $\gamma_0 = \gamma_0^{min}$ in time T with rate $r < 0$. Other parameters are: $\alpha = 0.3$, $\beta = 1$, $h = 0.4$. The seven cases correspond to the high-dimensional networks listed in Tab. S1. The solid curves are from Eq. (5).

4. Probability of R-tipping with time-varying parameters κ and γ_0

To extend our investigation into R-tipping in mutualistic networks with respect to the time rate of change of a single parameter, we study the effects of multiple time-varying parameters under the scenario where the species decay rate (κ) exhibits a linear increase and the mutualistic interaction strength (γ) simultaneously undergoes a linear decrease, so as to gain insights into how adverse environmental changes can impact the tipping probability and the overall stability of the mutualistic network. Specifically, we assume that κ increases linearly with time at the rate r_κ from a minimal value $\kappa_{\min}$ to a maximal value $\kappa_{\max}$ and γ_0 decrease linearly with time at the rate r_γ from a maximal value $\gamma_0^{\max}$ to a minimal value $\gamma_0^{\min}$:

$$\dot{\kappa}_j = \begin{cases} r_\kappa & \text{if} \quad \kappa_{\min} < \kappa_j < \kappa_{\max} \\ 0 & \text{otherwise,} \end{cases} \qquad [6]$$

$$\dot{\gamma}_0 = \begin{cases} -r_\gamma & \text{if} \quad \gamma_0^{\min} < \gamma_0 < \gamma_0^{\max} \\ 0 & \text{otherwise.} \end{cases} \qquad [7]$$

The time required for the parameter κ change is $T_\kappa = (\kappa_{max} - \kappa_{min})/r_\kappa$, where $r_\kappa > 0$ and the time required for the parameter γ_0 change is $T_{\gamma_0} = (\gamma_0^{min} - \gamma_0^{max})/r_{\gamma_0}$, where $r_{\gamma_0} < 0$.

To examine the probability of R-tipping, we set $r_\kappa = \mathcal{C} r_\gamma$, where $\mathcal{C} > 0$ and study three distinct scenarios by varying the parameter $\mathcal{C}$: $\mathcal{C} < 1$, $\mathcal{C} = 1$, and $\mathcal{C} > 1$. Using an analysis similar to the one in the main text, the probability of R-tipping is

$$\Phi(r) = B \exp\left[-C(\max(T_\kappa, T_{\gamma_0}))\right] \qquad [8]$$

with $B > 0$ and $C > 0$ being two fitting constants. Table S1 lists the parameter configurations and the corresponding values of the two fitting parameters for the ten high-dimensional empirical mutualistic networks.

Table S2. Empirical mutualistic networks, ranges of time-varying parameters κ and γ_0, and the fitting constants in Eq. (8)

Network	κ-interval	γ_0-interval	$\mathcal{C} < 1$ $[B,\ C]$	$\mathcal{C} = 1$ $[B,\ C]$	$\mathcal{C} > 1$ $[B,\ C]$
M_PL_008	[0.90 0.93]	[0.96 1]	[0.28, 0.60]	[0.28, 0.20]	[0.30, 0.10]
M_PL_013	[0.86 0.97]	[0.96 1]	[0.30, 0.40]	[0.29, 0.15]	[0.30, 0.18]
M_PL_022	[0.87 0.89]	[0.96 1]	[0.76, 0.29]	[0.77, 0.03]	[0.77, 0.02]
M_PL_023	[0.90 0.92]	[0.96 1]	[0.37, 0.52]	[0.37, 0.07]	[0.37, 0.03]
M_PL_027	[0.90 0.91]	[0.96 1]	[0.08, 0.72]	[0.09, 0.13]	[0.08, 0.02]
M_PL_032	[0.87 0.96]	[0.96 1]	[0.49, 0.25]	[0.49, 0.12]	[0.49, 0.10]
M_PL_036	[0.82 0.85]	[0.96 1]	[0.30, 0.42]	[0.29, 0.09]	[0.29, 0.01]
M_PL_037	[0.86 0.89]	[0.96 1]	[0.16, 0.55]	[0.16, 0.15]	[0.16, 0.05]
M_PL_038	[0.86 0.92]	[0.96 1]	[0.26, 0.45]	[0.26, 0.13]	[0.26, 0.11]
M_PL_045	[0.93 0.94]	[0.96 1]	[0.02, 0.65]	[0.02, 0.12]	[0.02, 0.05]

The probability of R-tipping in various scenarios for each network listed in Table S2 is shown in Figs. S5-S14, respectively. These results provide a detailed illustration of the tipping probabilities for ten high-dimensional empirical mutualistic networks under the different parameter settings, where each figure corresponds to a specific network.

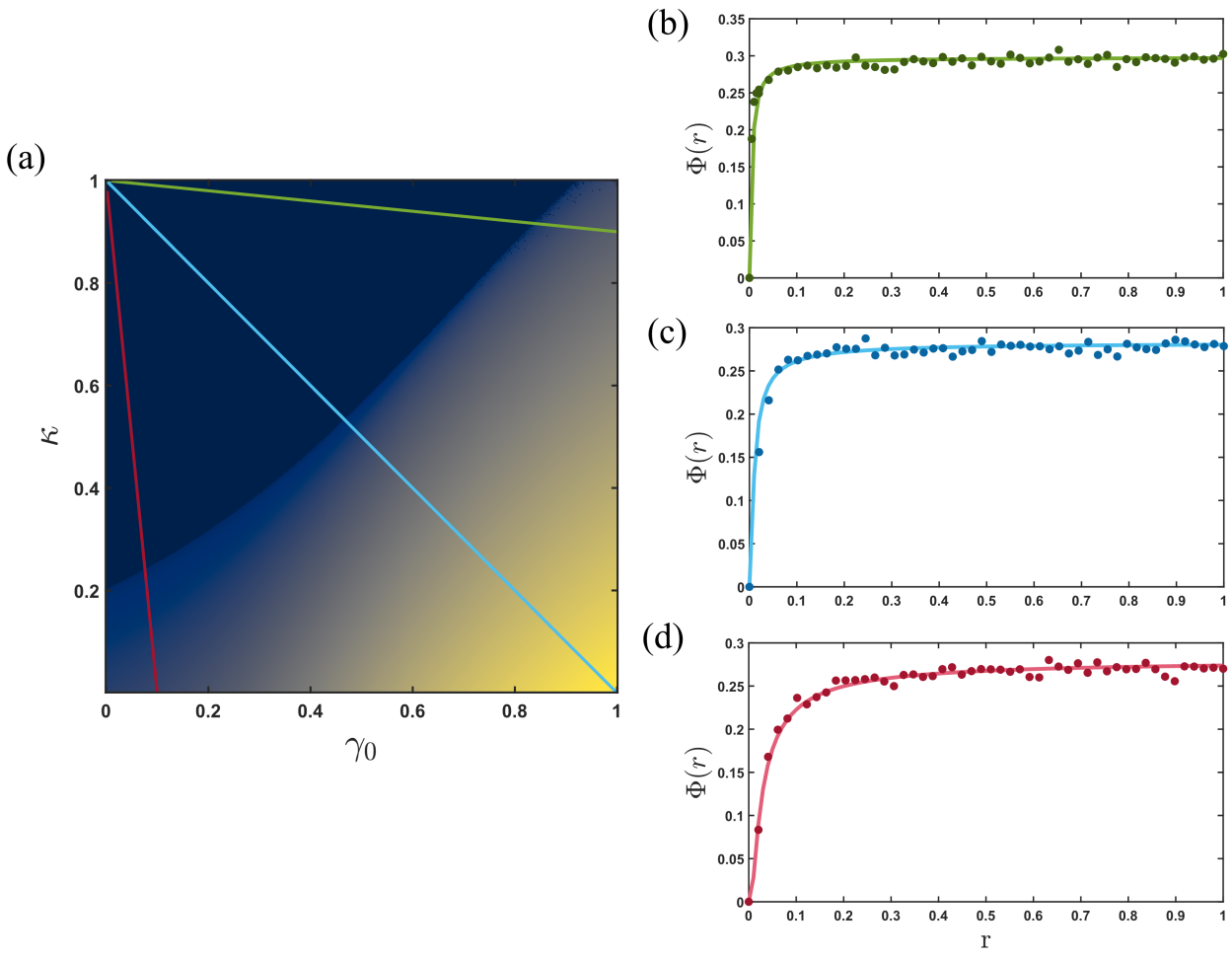

Fig. S5. Scaling law of probability of R-tipping in two-dimensional parameter space for the empirical network M_PL_008. (a) Two-dimensional parameter plane of the species decay rate (κ) and the mutualistic interaction strength (γ_0). The solid lines correspond to the three different scenarios of the parameter $\mathcal{C}$ in calculating the probability of the R-tipping point using 10^5 initial conditions: (b) $\mathcal{C} < 1$, (c) $\mathcal{C} = 1$, and (d) $\mathcal{C} > 1$. The initial parameter values are $\gamma_0 = \gamma_0^{max}$ and $\kappa_0 = \kappa_{min}$, and they change linearly with time to $\gamma_0 = \gamma_0^{min}$ and $\kappa_0 = \kappa_{max}$, respectively. Other parameter values are $t = 0.5$, $\beta = 1$, $\alpha = 0.3$, $\mu = 0$, and $h = 0.5$.

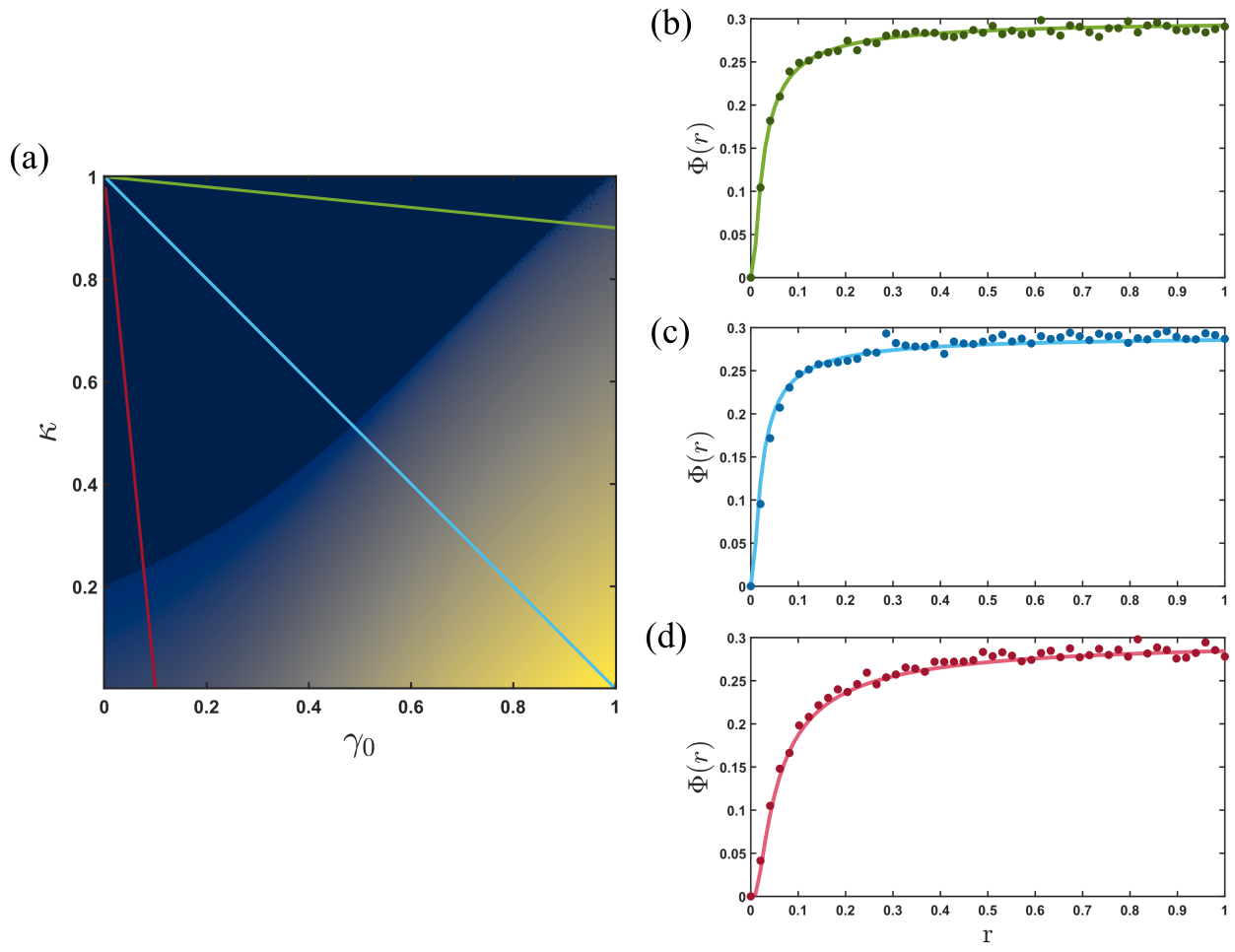

Fig. S6. Scaling law of probability of R-tipping in two-dimensional parameter space for the empirical network $\mathrm{M\_PL\_013}$. Legends are the same as those in Fig. S5 except $h = 0.4$.

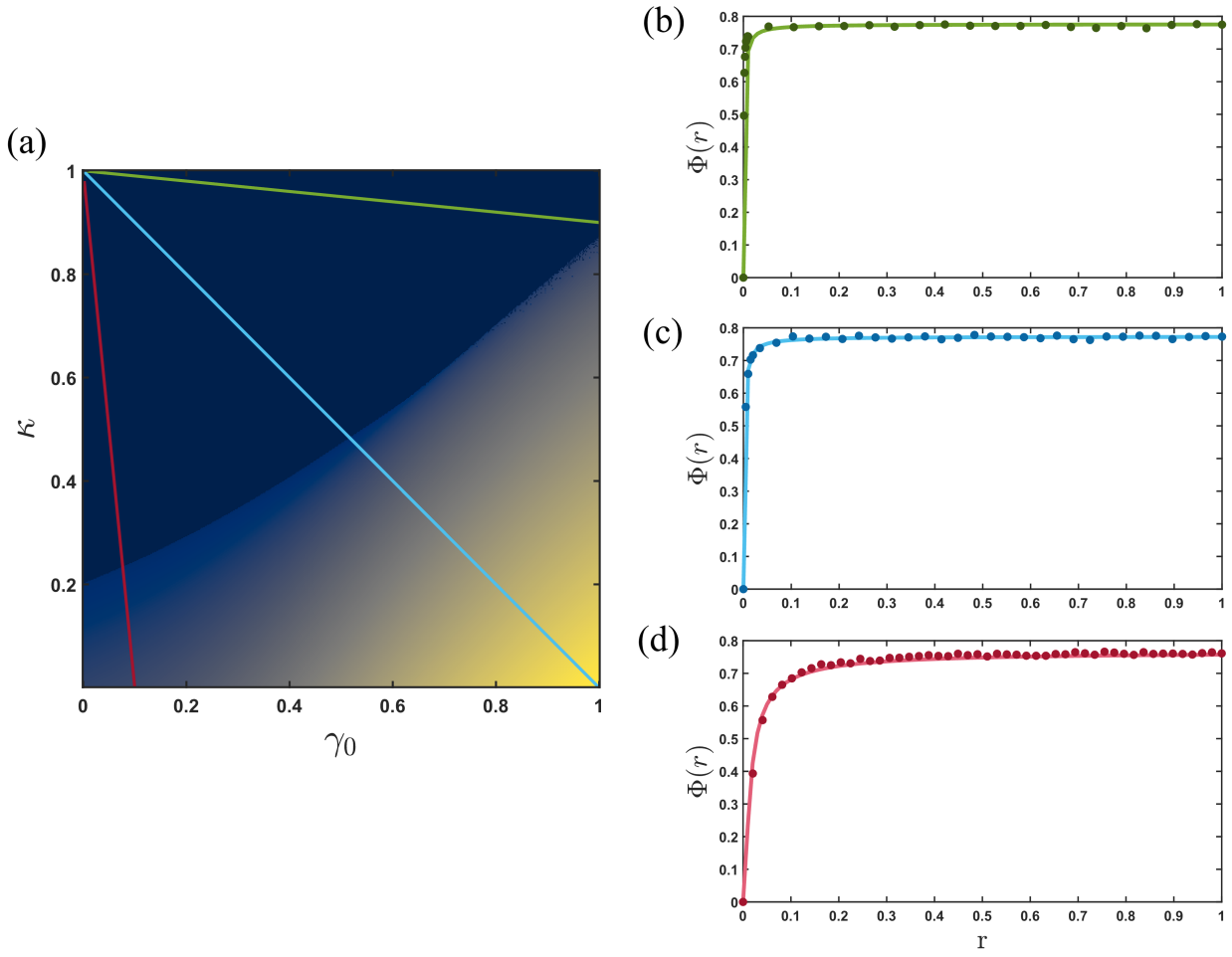

Fig. S7. Scaling law of probability of R-tipping in two-dimensional parameter space for the empirical network $\mathrm{M\_PL\_022}$. Legends are the same as those in Fig. S5 except $h = 0.35$.

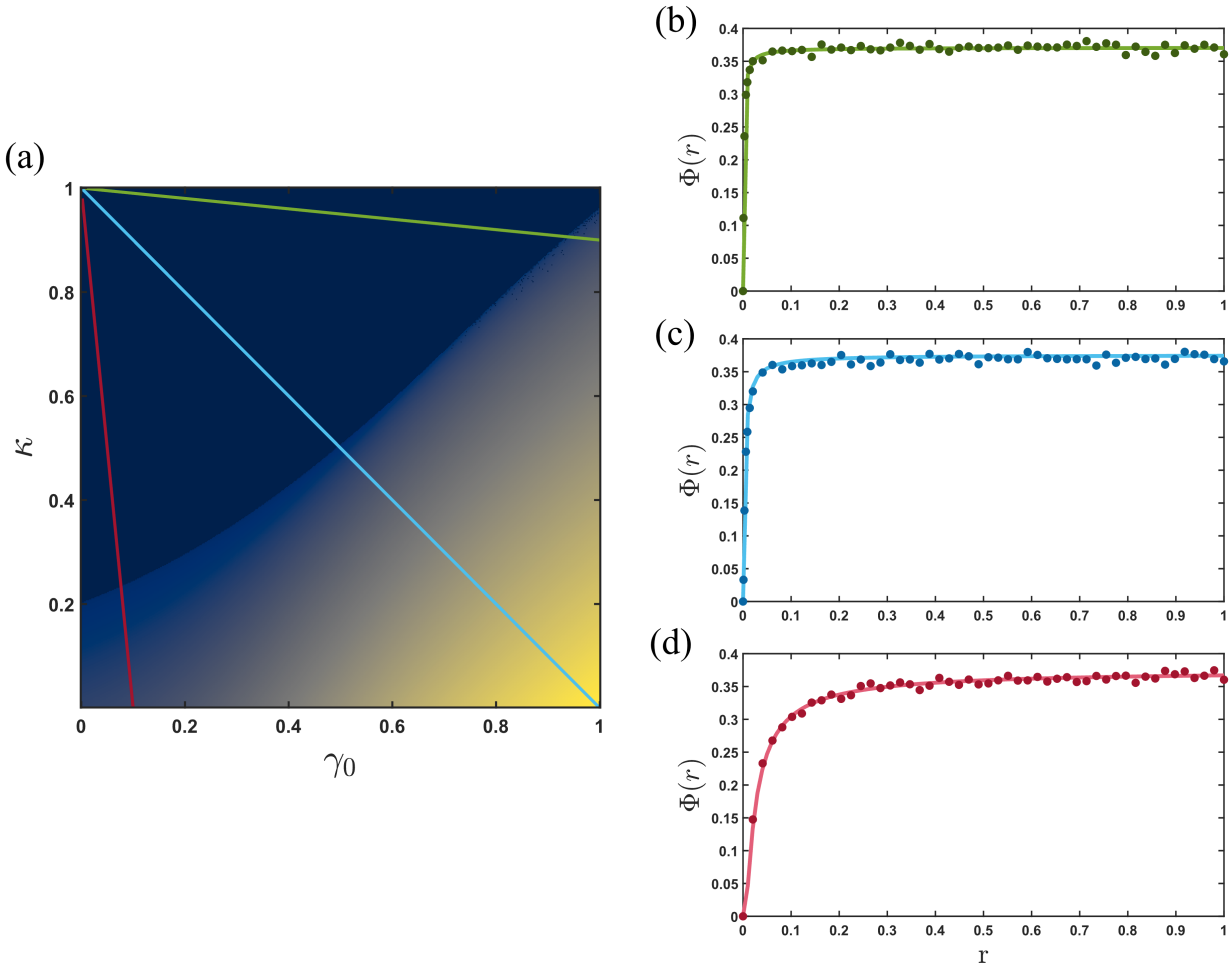

Fig. S8. Scaling law of probability of R-tipping in two-dimensional parameter space for the empirical network $\mathrm{M\_PL\_023}$. Legends are the same as those in Fig. S5 except $h = 0.4$.

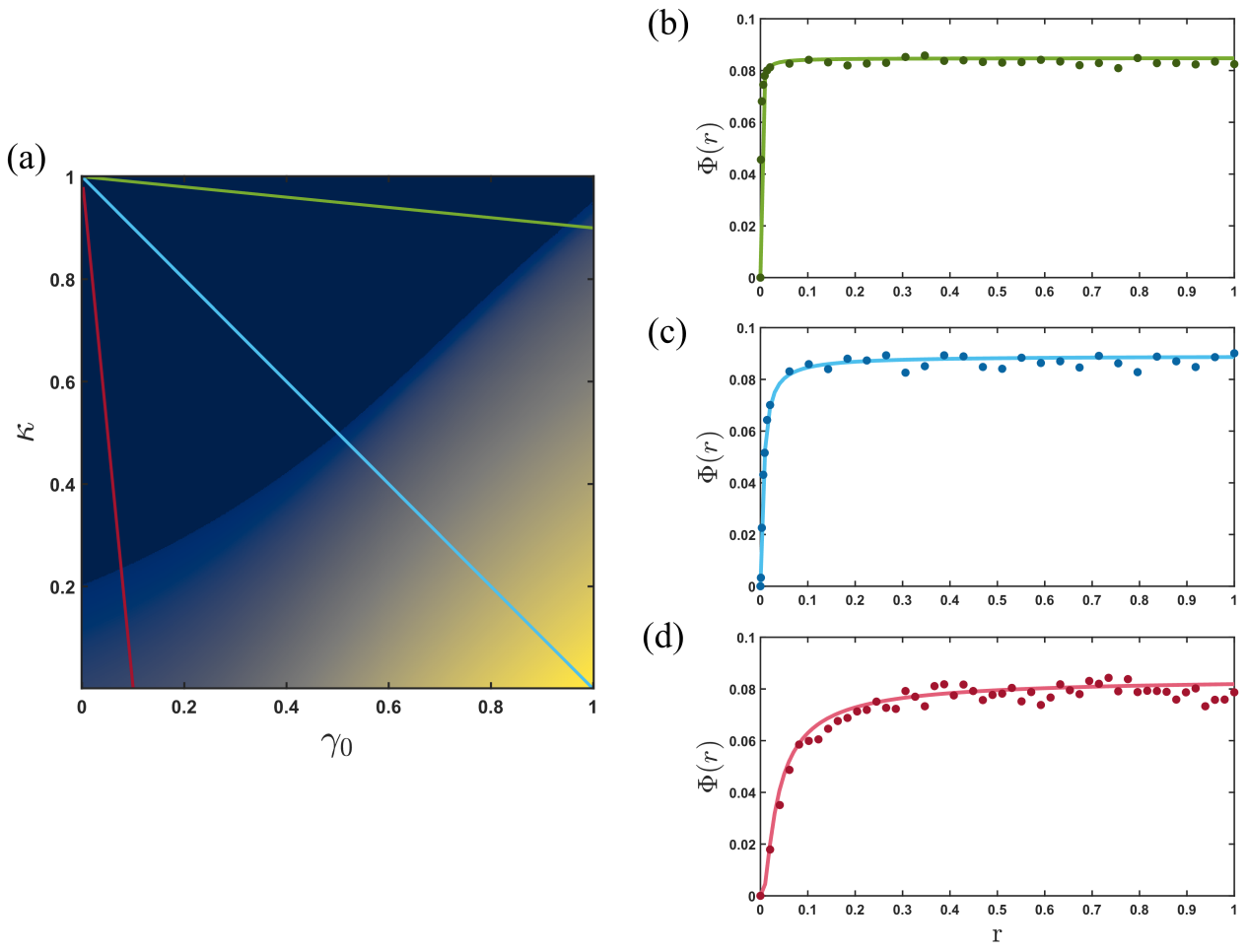

Fig. S9. Scaling law of probability of R-tipping in two-dimensional parameter space for the empirical network M_PL_027. Legends are the same as those in Fig. S5.

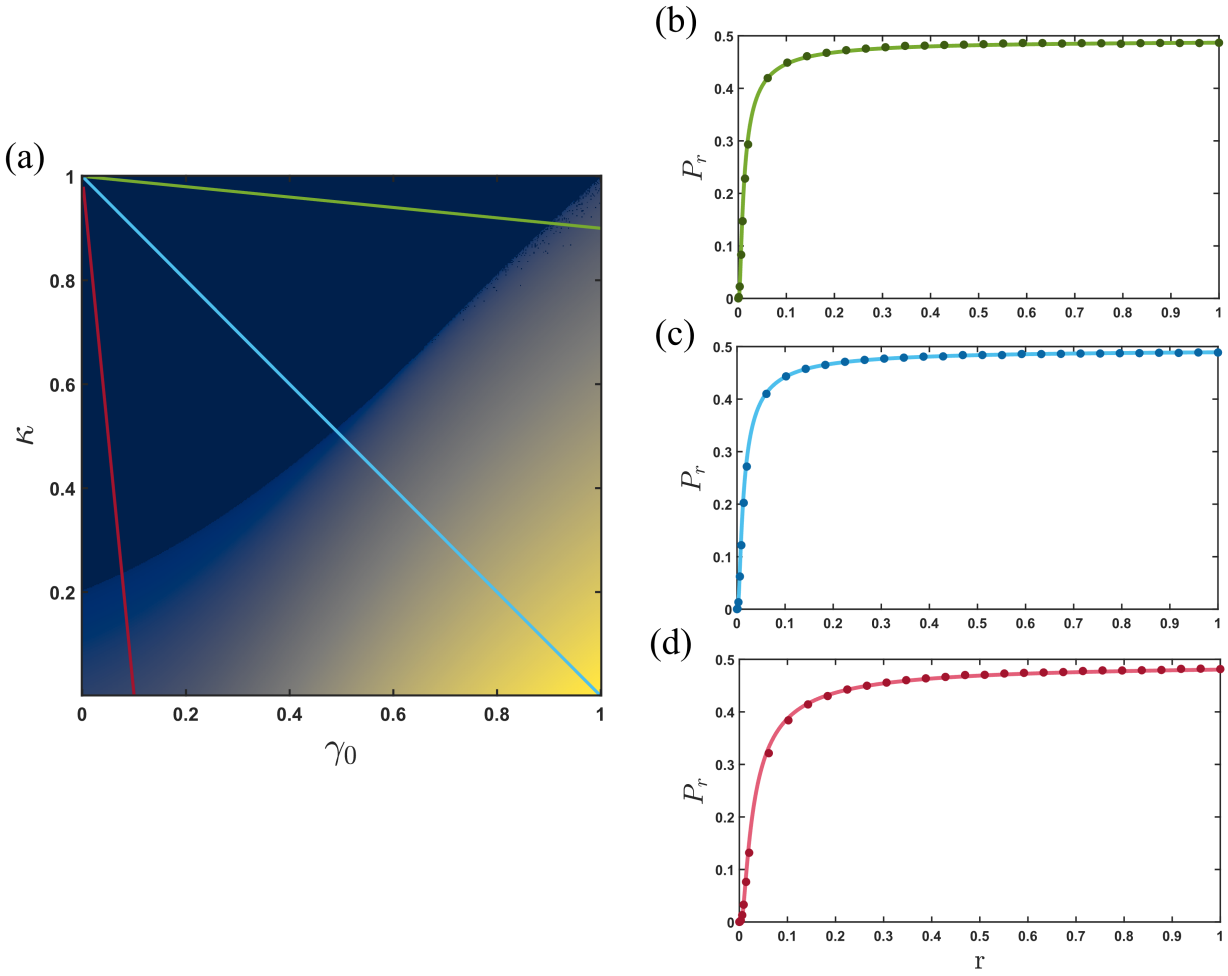

Fig. S10. Scaling law of probability of R-tipping in two-dimensional parameter space for the empirical network $\mathrm{M\_PL\_032}$. Legends are the same as those in Fig. S5.

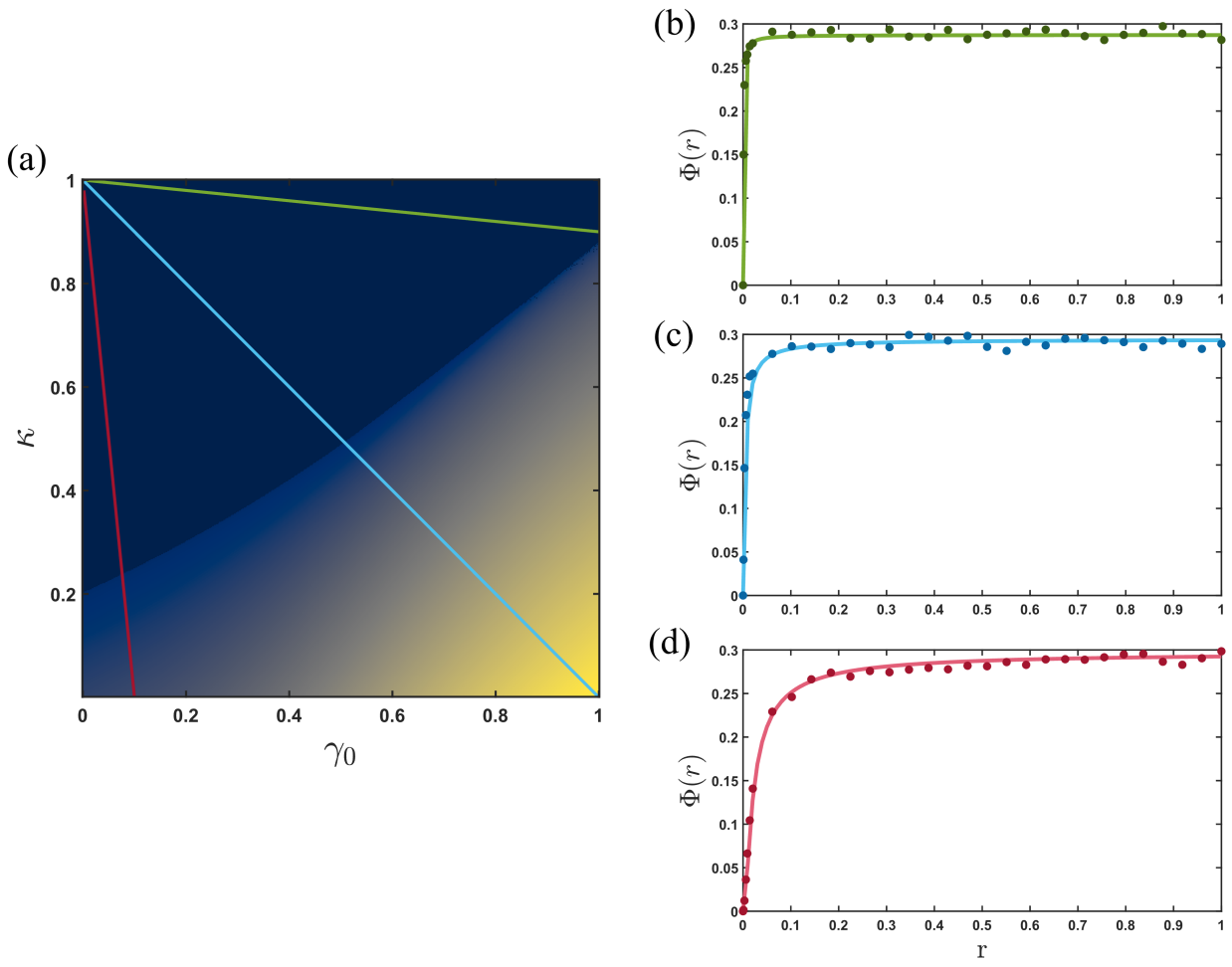

Fig. S11. Scaling law of probability of R-tipping in two-dimensional parameter space for the empirical network $\mathrm{M\_PL\_036}$. Legends are the same as those in Fig. S5.

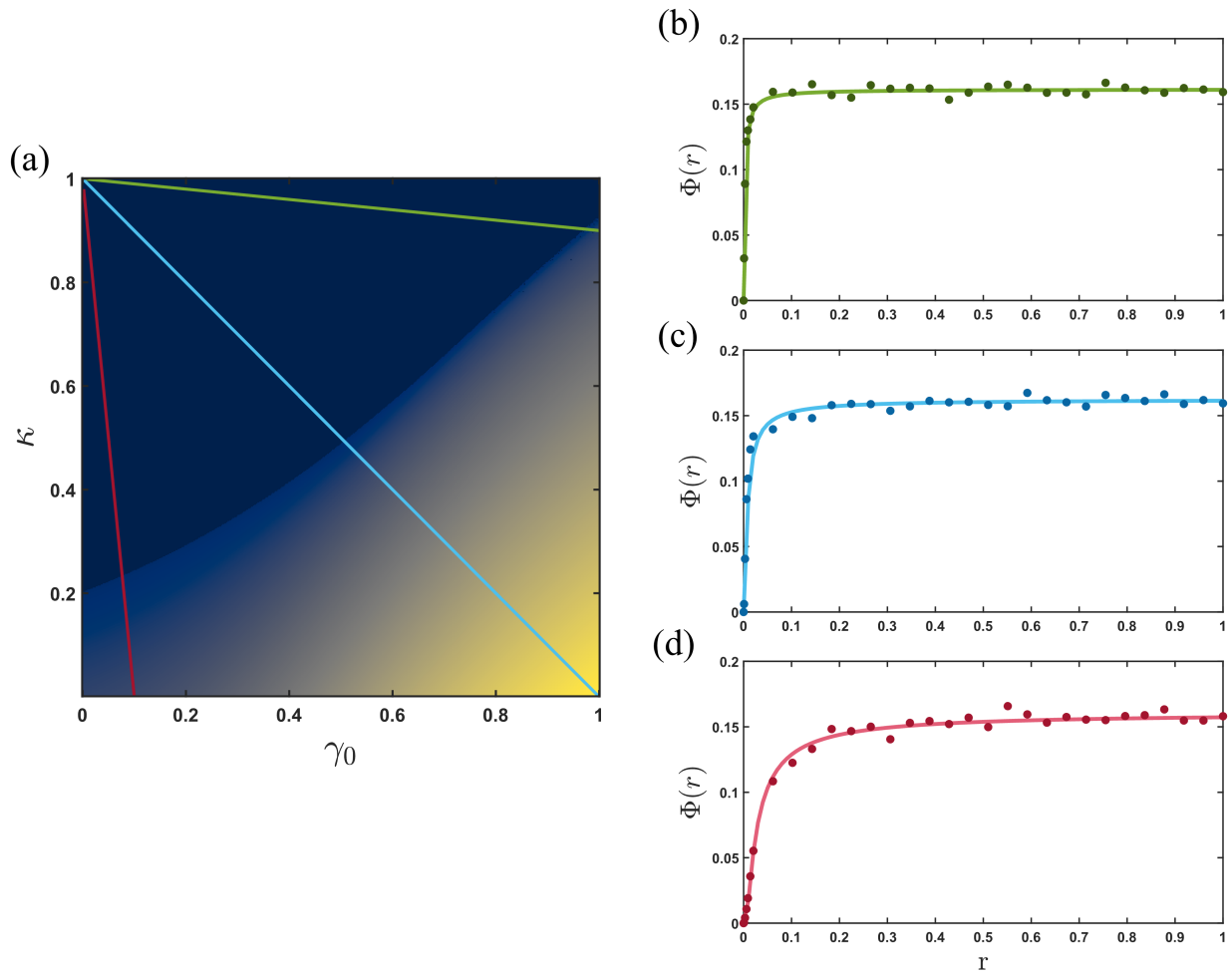

Fig. S12. Scaling law of probability of R-tipping in two-dimensional parameter space for the empirical network $\mathrm{M\_PL\_037}$. Legends are the same as those in Fig. S5.

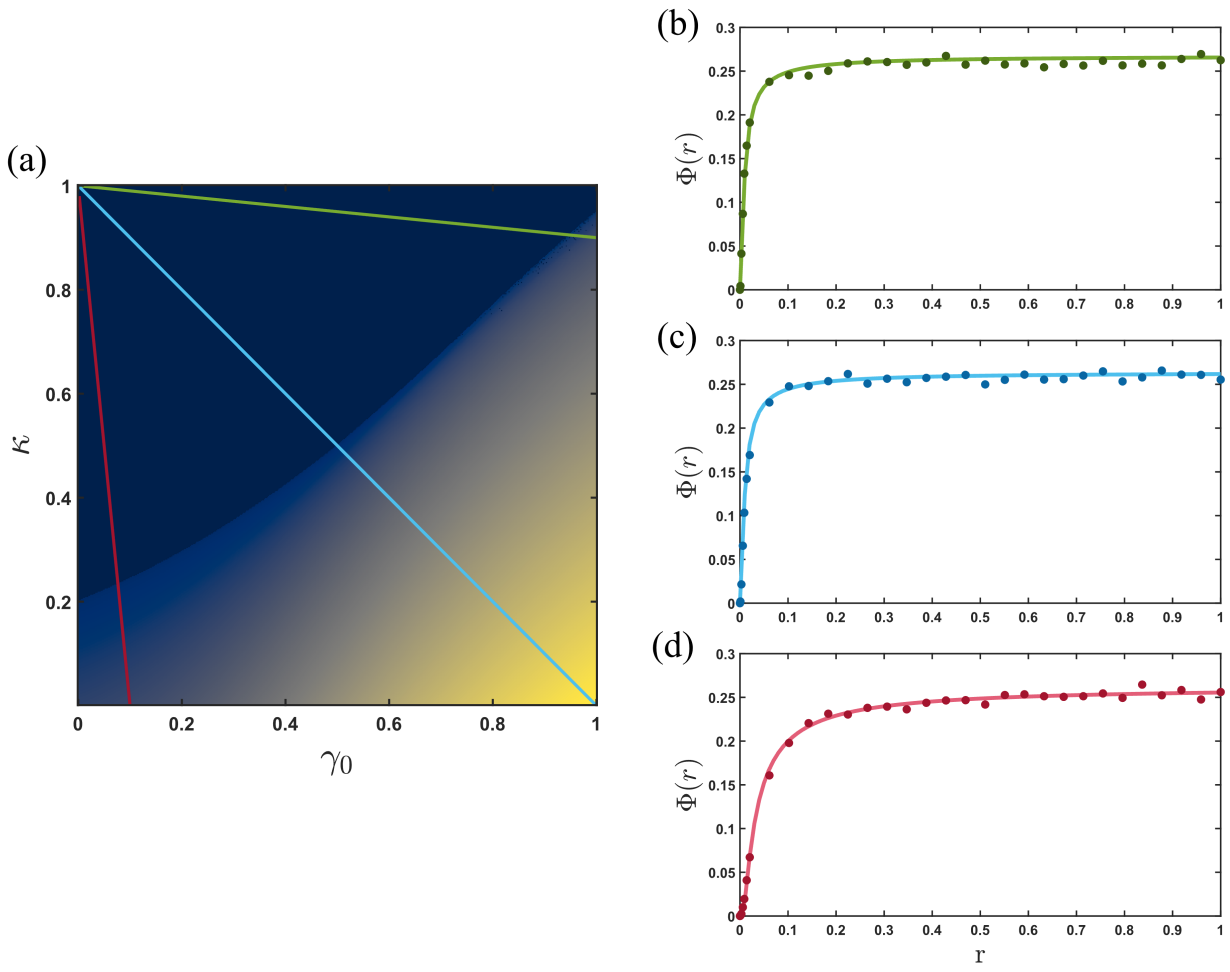

Fig. S13. Scaling law of probability of R-tipping in two-dimensional parameter space for the empirical network $\mathrm{M\_PL\_038}$. Legends are the same as those in Fig. S5.

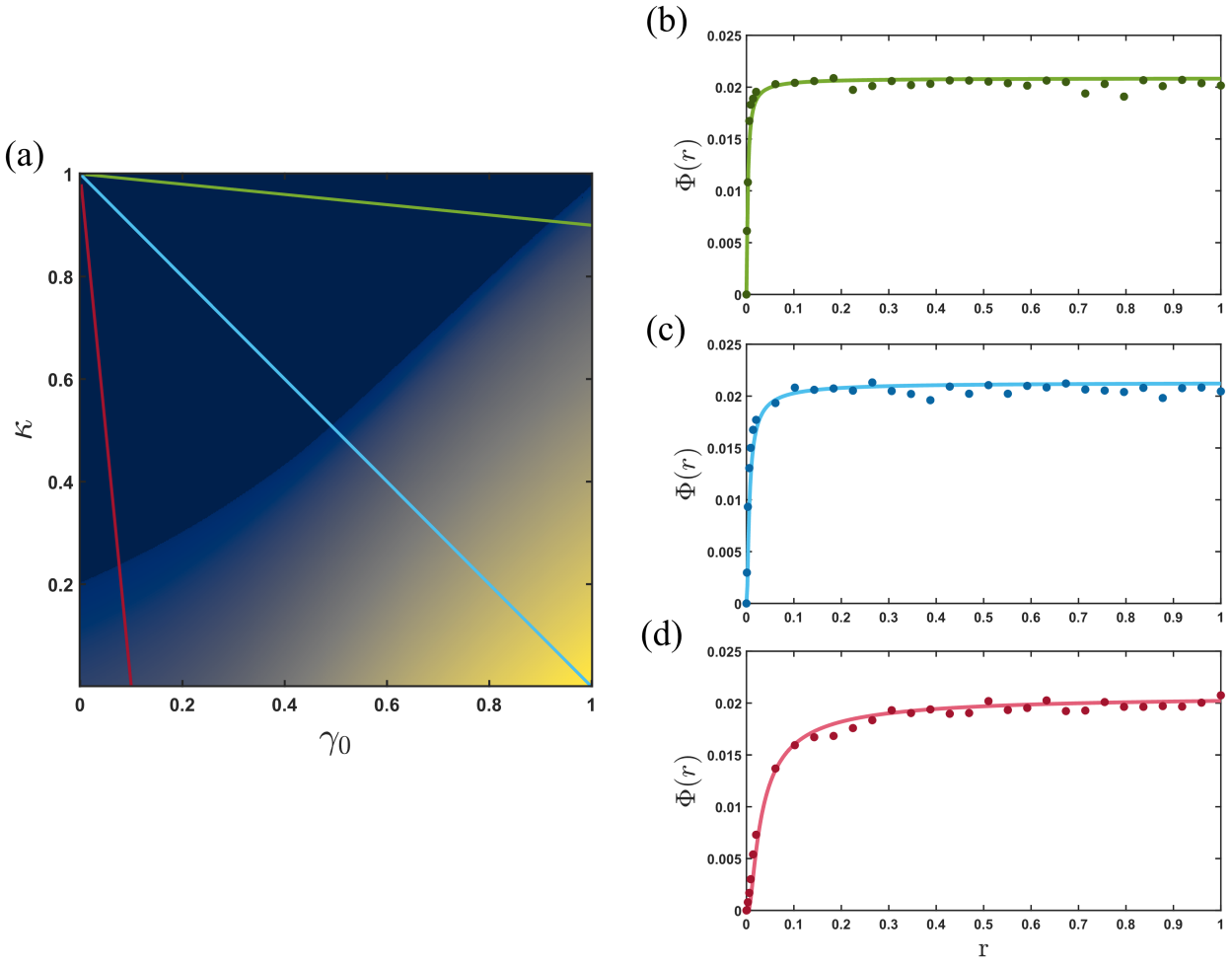

Fig. S14. Scaling law of probability of R-tipping in two-dimensional parameter space for the empirical network M_PL_045. Legends are the same as those in Fig. S5.

References

1. Junjie Jiang, Zi-Gang Huang, Thomas P Seager, Wei Lin, Celso Grebogi, Alan Hastings, and Ying-Cheng Lai. Predicting tipping points in mutualistic networks through dimension reduction. *Proc. Nat. Acad. Sci. (UsA)*, 115(4):E639–E647, 2018.